frontiers | Frontiers in Energy Research

TYPE Technology and Code
PUBLISHED 08 January 2024
DOI 10.3389/fenrg.2023.1257050

OPEN ACCESS

EDITED BY
Foo Yi Shyh Eddy,
Nanyang Technological University,
Singapore

REVIEWED BY
Parikshit Pareek,
Los Alamos National Laboratory (DOE),
United States
K. Ramya,
Sri Sairam College of Engineering, India

*CORRESPONDENCE
Mackenzie Robert Wodicker,
mwodicke@asu.edu

RECEIVED 11 July 2023
ACCEPTED 04 December 2023
PUBLISHED 08 January 2024

CITATION
Wodicker MR, Nelson J and Johnson NG (2024), Unified dispatch of grid-connected and islanded microgrids. *Front. Energy Res.* 11:1257050. doi: 10.3389/fenrg.2023.1257050

Unified dispatch of grid-connected and islanded microgrids

Mackenzie Robert Wodicker*, James Nelson and Nathan Gregory Johnson

The Polytechnic School, Ira A. Fulton Schools of Engineering, Arizona State University, Mesa, AZ, United States

This work develops microgrid dispatch algorithms with a unified approach to model predictive control (MPC) to (a) operate in grid-connected mode to minimize total operational cost, (b) operate in islanded mode to maximize resilience during a utility outage, and (c) utilize weighting factors in the grid-connected objective function to preserve islanded capability (on-site fuel reserves, battery state of charge) to enhance resilience in the potential event of an unplanned grid outage. Resilience is defined using microgrid survivability (probability to serve 100% of critical load), autonomy (duration of time to serve 100% of critical load), and unserved energy (curtailed critical load) for a target of 7 days during a grid outage. The developed methods are applied to a military microgrid with 2,250 kW of diesel generation, 3,450 kW/13,800 kWh battery storage, and 16,479 kW of solar photovoltaics. Sensitivity analysis is conducted to determine the selection of weighting factors to have the best impact on three developed objectives: grid-connected economics, islanded resilience, and carbon intensity. Optimal weighting factors reduce operating costs by 0.1%, increase survivability by 3.9%, increase autonomy by 16.7%, reduce unserved energy by 94.1%, and increase carbon intensity by 2.5%.

KEYWORDS

microgrid, climate resilience, microgrid islanding, optimization, microgrid dispatch, energy economics

1 Introduction

Climate change has increased the frequency and intensity of natural disasters (Cane et al., 1997; Anderson and Bausch, 2006) and caused significant damage to electrical infrastructure from severe weather (Bryan, 2012; Kerr, 2011; Stott, 2016) and forest fires (Sunrun Inc, 2019; Stelloh, 2019). The damage can create large-scale and prolonged outages with harmful impacts through loss of essential services such as hospitals, climate control, and transportation (Anderson and Bell, 2012), and may include increased impacts to rural communities and marginalized populations (UNISDR, 2015). Anthropogenic stressors such as physical and cyber-attacks (Chen et al., 2011; Zhu et al., 2014), lack of maintenance leading to equipment failure (Venkatasubramanian and Yuan, 2004), and human error (Muir and Lopatto, 2004) can also result in grid outages. These situations are characterized as high-impact, low-frequency (HILF) events that motivate attention to improve the resilience of critical power systems to anticipate, adapt, and recover from disturbances (Raoufi et al., 2020). These HILF events cause perturbations in the voltage, grid frequency, current flows, and rotating generator torque that can cascade beyond the immediate location of the fault

and affect adjacent infrastructure and regions. Mitigation strategies to address these stability issues include distributed control strategies (Lee et al., 2016; Ayar et al., 2017), generator control circuits (Ellithy et al., 2013; Derafshian and Amjady, 2015), fast-acting power electronics devices (Ma et al., 2016; Yu et al., 2018), and distributed energy resources (DERs) and microgrids (Krismanto et al., 2021). Areas of the grid with high amounts of renewable generation and DERs may be at higher risk to outages if the variability in their output power is not complemented with advanced power electronics or sufficient operating reserves from storage, controllable loads, and dispatchable generation (Ogunjuyigbe et al., 2016; Khani et al., 2012; Dulău et al., 2014; Resource and MW Fault Induced Solar Photovoltaic, 2017).

These centralized approaches to grid stability are increasingly effective but still cannot guarantee resilience to critical loads if transmission and distribution lines are severed. Critical circuits at hospitals, military bases, cellular towers, refrigeration, data centers, and other uses are often equipped with an uninterruptable power source (UPS) and generators to maintain power in the event of a grid outage. It is less common to have a coordinated set of renewables, storage, generators, and load control that serves an entire distribution network behind-the-meter as a district or campus-scale microgrid (Zheng, 2022; Energy Government and US, 2022). Grid-connected microgrids are an existing technology with a rapidly growing adoption trend to provide resilience to customers requiring power in the event of a grid outage. The U.S. Department of Energy (DOE) defines a microgrid as "*a group of interconnected loads and distributed energy resources within clearly defined electrical boundaries that acts as a single controllable entity with respect to the grid. A microgrid can connect and disconnect from the grid to enable it to operate in both grid-connected or island-mode*" (Ton and Smith, 2012).

Microgrids can provide value in grid-connected mode and in islanded mode. During grid-connected operation, microgrids can provide cost-savings through dispatch of DERs to reduce energy purchases, reduce demand charges, and shift power use to lower cost time-of-use (TOU) periods (Thompson et al., 2016; Nelson and Johnson, 2020; Palma-Behnke et al., 2011; Miao et al., 2013). Additional cost savings can be secured by revenue curation through participation in wholesale energy and ancillary service markets by selling electricity at real-time prices. Federal Energy Regulatory Commission (FERC) Order No. 2222 enables DERs and DER aggregators to participate in real-time markets (Cano, 2020). These microgrid assets require coordination to gain the most value, with typical approaches to economic dispatch including logic-based control (Theerthamalai and Maheswarapu, 2010; Ton and Smith, 2012), non-linear optimization (Bhattacharjee and Khan, 2018), dynamic systems theory (Xiaoping et al., 2010), multi-objective optimization (Meiqin et al., 2010), and Model Predictive Control (MPC) (Nelson and Johnson, 2020; Nelson et al., 2020). This paper uses MPC to dispatch energy assets amidst uncertainty (e.g., variability in renewable generation and loads) (Rawlings and Mayne, 2009) and enhance the technical and economic metrics for microgrids (Bruni et al., 2014). MPC uses historical data and real-time forecasting of future system states to identify optimal decisions for asset dispatch that satisfy the goals of an objective function such as least cost operation, highest resilience, or lowest carbon (Nelson and Johnson, 2020; Nelson et al., 2020). MPC uses static asset parameters and time series data such asset status, critical and controllable load status, solar insolation and wind speed, ambient air temperatures, retail energy and demand charge costs, and market pricing signals to determine the optimal operation of a microgrid (Nelson and Johnson, 2020; Xiaoping et al., 2010; Meiqin et al., 2010). Renewables and energy storage are increasingly common in microgrids, and help organizations meet carbon reduction goals while also reducing electricity bills and enhancing resilience (Theerthamalai and Maheswarapu, 2010; Bhattacharjee and Khan, 2018).

Microgrids provide resilience to critical loads in the event of electric utility outages (Energy Government and US, 2022; Moretti et al., 2019; Rawlings and Mayne, 2009; Nelson et al., 2020). Back-up power is presently common to maintain critical loads for public health services, fire and police, and military bases, to name a few, and recent changes in technology, business models, and regulation are opening the door for microgrids to displace back-up generators. Not only this, but distribution system infrastructure can be damaged during utility outages, causing sizable economic impacts and motivating microgrids to enhance system stability in the larger grid (Energy Government and US, 2022).

The increasing focus on resilience has not yet led to a single commonly accepted definition or quantifiable metric for resilience. The term generally refers to the ability of a system to withstand HILF events (Raoufi et al., 2020; Bhusal et al., 2020). Some examples of quantitative metrics include Customer Average Interruption Duration Index (CAIDI), Loss of Load Frequency (LOLF), Loss of Load Probability (LOLP), asset reliability, loss of power to critical public service loads such as emergency management and hospitals, power quality, and economic losses from a grid outage (Raoufi et al., 2020; Khan and Iravani, 2007; Fu et al., 2015; Bhusal et al., 2020). In this paper, the metric of *survivability* is used from (Nelson et al., 2020) to describe the resilience of microgrid operations as a probability that critical load on the system will be served during islanded conditions. The quantitative development is similar to LOLP, which uses uncertainties in load forecasts to determine the probability that the peak load on a power system will exceed the generating capacity (Gambirasio, 1976). Survivability, however, uses failure rates of generating assets and considers all possible system configurations to determine the probability that generation can meet the critical load. *Autonomy* is also used to describe the duration of time the microgrid can meet critical loads while islanded. *Unserved energy* to critical loads is reduced and eliminated through microgrid control operations. These metrics are used to evaluate the resilience of MPC approaches developed in this paper.

The objective function for microgrid operation is different in grid-connected mode (economic optimization) and in islanded mode (resilience optimization) and asset dispatch must adapt accordingly. For example, a microgrid's primary objective may be to provide 7-day autonomy and therefore microgrid assets will be dispatched to ensure energy is available for an islanding event (Johnson, 2022). Conversely, a commercial project may have an interest in electricity cost savings resulting in higher energy market participation and energy and demand charge reduction during peak TOU periods (Wood, 2022). Motivation exists, especially for large customers, to optimize both resilience and economic impacts of microgrid operations. Most current literature does not investigate the interrelated influence of grid-connected microgrid economic

dispatch with the resilience of the microgrid during islanded operation, instead, those operating modes are isolated and approached separately (Nelson and Johnson, 2020; Nelson et al., 2020; Jafari et al., 2018). Efforts in this paper show the benefits for co-optimization of grid-connected and islanded algorithms. Minimal to no research exists on how economic optimization for grid-connected operations affects resilience optimization for islanded operations. This paper attempts to address this gap by coupling microgrid dispatch approaches presented in (Nelson and Johnson, 2020; Nelson et al., 2020), in which MPC and Markov Chains are used to dispatch microgrids and quantify resilience during islanded operations, respectively. By coupling the methods of grid-connected and islanded dispatch of microgrids, the study shows the intersectional relationship between cost-minimized grid-connected cost and resilience-maximized dispatch during unpredictable utility outages. Additionally, this work adopts the use of objective function weighting factors from (Nelson et al., 2020) for islanded dispatch and applies them to grid-connected dispatch methods in (Nelson and Johnson, 2020) in an effort to improve islanded resilience while maintaining low operational cost. This work identifies that microgrid generator and battery usage is the key factor in managing this intersectional relationship of cost and resilience, and presents a method to optimize usage for the best overall outcome. Contributions of this work to literature include:

- Introduces objective functions and demonstrates how microgrid control decisions in grid-connected and islanded mode can be coordinated to advance overall economic and resilience goals;
- Demonstrates and studies the relationship between grid-connected operational cost and islanded resilience of microgrid operations;
- Enhances resilience quantification by incorporating solar photovoltaic (PV) reliability into microgrid survivability calculations;
- Identifies control parameters to optimize microgrid behavior with respect to grid-connected economics and islanded resilience, with an associated quantification of environmental impact to meet carbon reporting goals.

2 Materials and methods

2.1 Microgrid dispatch formulations

The MPC approach implements a Mixed-Integer Linear Programming (MILP) optimization formulation with static and time series data to calculate optimal dispatch decisions. MPC uses a receding time horizon of static length that contains relevant forecasted data (electrical load, solar PV output, grid electricity pricing signals) to make informed decisions for current operations and plan future operations. The first control action within the time horizon is the executed action and is selected with consideration of potential system states in the remaining time steps of the MPC time horizon. One time step is advanced and the MPC is repeated, and this process is continued through the duration of the simulation timeframe.

A Python-based simulation environment was developed to simulate dispatch of microgrid assets in both grid-connected and islanded modes. It is crucial to dispatch microgrid assets to improve economics without sacrificing microgrid survivability, or at least, evaluating the impact of grid-connected dispatch decisions on microgrid survivability in the event a grid outage occurs at any time. These tertiary control signals are used to optimize minute-to-minute performance of a microgrid over the course of a longer-term planning period. The sub-second switching sequences and associated changes in primary controls of power hardware required to transition from grid-connected to islanded mode are outside the scope of this study. Figure 1 shows the process flow to simulate operations of a microgrid and how data is shared between grid-connected and islanded operating modes.

2.2 Grid-connected dispatch

Grid-connected dispatch algorithms control use of batteries, fossil fuel generators, and solar PV to reduce utility costs by lowering energy charges, lowering demand charges, and generating revenue through energy sales. The grid-connected objective function seeks to minimize operating costs consisting of a generator term, battery term, utility energy import/export term, and demand charge term. Generator operating cost is represented by fuel cost, C_{gen}^{fuel}. Generator efficiency is represented by the term η_{gen} (calculated using $\rho_{gen} \times LHV_{fuel}$). Fixed and variable generator O&M costs could be added to the grid-connected objective depending on contractual agreements with the developer to account for hourly labor costs or runtime maintenance cost. In this case, however, maintenance is annualized at a fixed cost and does not vary with operations, and thus is not captured in the objective function. Variable battery O&M costs, $C_{bat}^{OM,v}$, are incurred through charging and discharging of battery stacks. The variable battery O&M captures the cost of the degradation of the battery stacks through cycling, and represents the cost to replace them over the system lifetime. Solar PV fixed and variable O&M costs are not included in the objective function due to annualized O&M cost by contractual agreement and hence do not affect dispatch. In some other cases, variable solar O&M could be captured in the O&M to account for replacement cost of solar PV and could influence whether PV is curtailed. Utility per-unit energy purchase cost and sales price are represented as $C_{grid,t}^{b}$ and $C_{grid,t}^{s}$, respectively, and change based on the TOU period according to the time step, t. The time step variable increments forward in time from the start of the simulation period to the end of a simulation period, for example, from 1 to 8,760 for a year-long simulation with hourly time steps. The variable $C_{grid,t}^{s}$ is set to the utility's annual purchase rate for overgeneration and is typically the average annual wholesale energy rate, as assumed here. For the economic optimization in a net metering agreement, the generated solar PV is used to offset energy purchases at the retail tariff rate, which is higher than the wholesale energy rate that would be counted as revenue if excess is sold to the utility. There is a potential, in this formulation, to undervalue the net metering benefit because the MPC time horizon is only 7 days long and does not consider moving excess energy across longer time horizons such as a month or a year which are typical for net metering billing cycles.

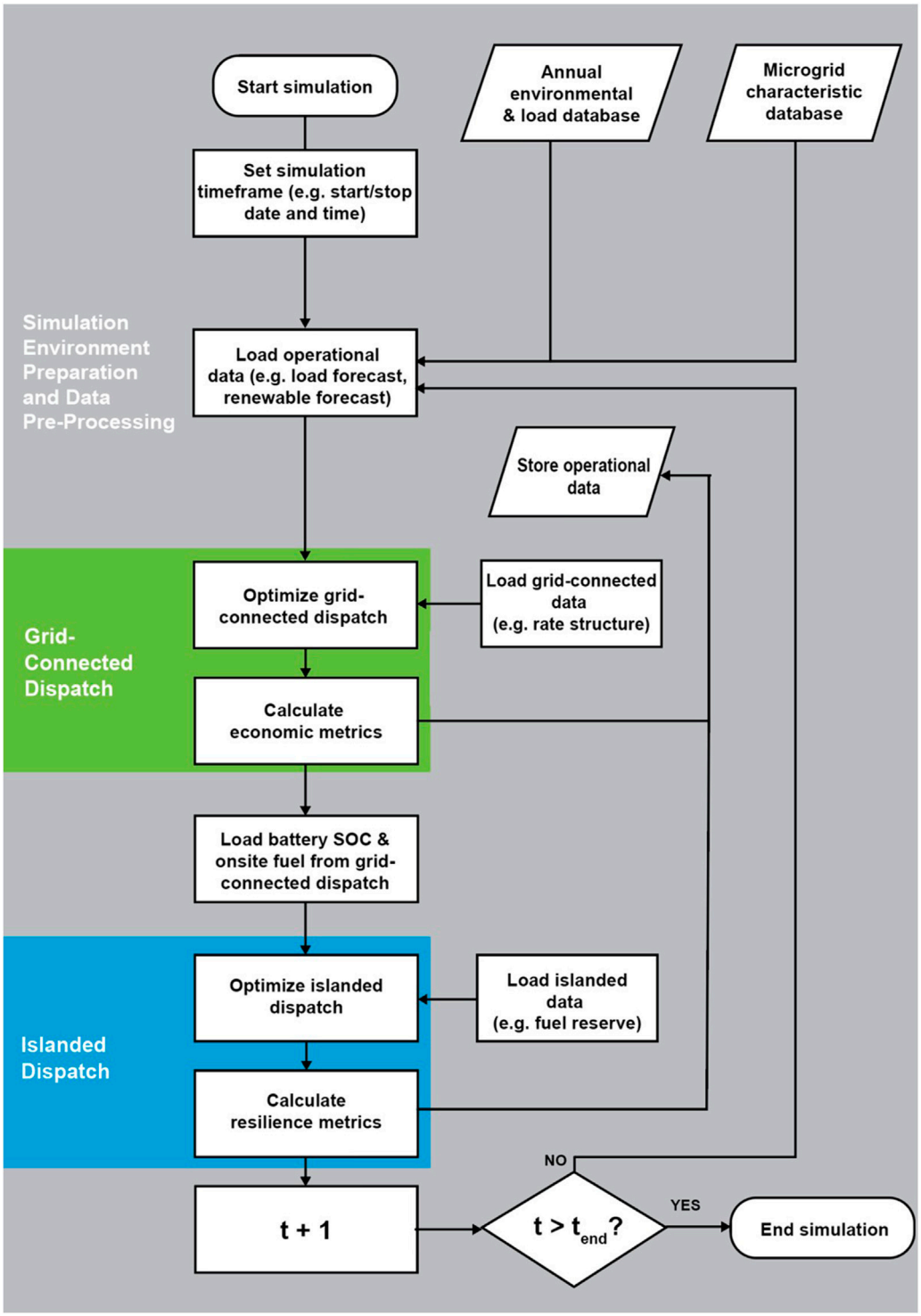

FIGURE 1
Process flow for simulating unified dispatch of microgrid operations.

A "time step hourly fraction", τ, is included in the formulation to account for the time resolution that simulations occur, and can be adjusted for 5-min, 15-min, 1-h, or other time step increments. Across each TOU period in the utility purchase agreement, peak demand charges are calculated by the product of the TOU demand price, $C_{grid,n}^{dem}$, with the period's peak kW demand, $P_{grid,n}{}^{max}$, and require an additional summation term to consider the demand charges across all TOU types included in the simulation time horizon (off-peak, mid-peak, on-peak, etc.). The TOU demand charges are scaled in the objective function by dividing total

10.3389/fenrg.2023.1257050

hours in the simulation time horizon, T_h, by total hours in the billing period, T_{bp}, to reflect demand charges that only represent a portion of the billing period. Eq. (1) shows the objective function to minimize operating costs for grid-connected microgrid dispatch. The set of constraints that govern microgrid behavior and interaction between decision variables in the optimization formulation are given in Appendix A.

$$J := \sum_{t=0}^{T_h} \left[\left(\sum_{\forall gen} \left(C_{gen}^{fuel} \times P_{gen,t} \times \eta_{gen} \right) + \sum_{\forall bat} \left(\left(C_{bat}^{OM,v} \times P_{bat,t}^{d} \right) + \left(C_{bat}^{OM,v} \times P_{bat,t}^{c} \right) \right) + \left(C_{grid,t}^{b} \times P_{grid,t}^{b} - C_{grid,t}^{s} \times P_{grid,t}^{s} \right) \right) \times \tau + \frac{T_h}{T_{bp}} \sum_{n=1}^{N_{TOU}} C_{grid,n}^{dem} \times {P_{grid,n}}^{max} \right] \quad (1)$$

2.3 Islanded microgrid dispatch

The islanded objective function in Eq. (2) consists of three primary terms with associated weighting factors ω_{load}, ω_{bat}, and ω_{fuel} to prioritize the corresponding term load, battery, and fuel reserve during optimization. The signs of each term indicate that energy stored in the battery is maximized, and fuel consumption and curtailed load are minimized. This formulation maximizes total reserve capacity from generators and batteries to mitigate effects of a potential asset failure, as initially demonstrated in (Nelson et al., 2020). Weighting factors sum to one, with ω_{load} set nearly equal to one (0.999999999) to heavily disincentivize load shedding, with ω_{fuel} set to 0.0 and ω_{bat} set to 0.000000001 as determined by sensitivity analysis in (Nelson et al., 2020) to maintain battery reserve capacity and improve microgrid survivability.

$$J := \sum_{t=0}^{T_h} \left[\omega_{fuel} \sum_{\forall gen} \left(P_{gen,t} \times \eta_{gen} \right) - \omega_{bat} \left(\frac{P_{bat}^{d,max}}{{E_{bat}}^{max}} \right) \sum_{\forall bat} \left(E_{bat,t} \right) + \omega_{load} \left(\frac{P_t^{slack}}{t+1} \right) \right] \quad (2)$$

2.4 Grid-connected microgrid dispatch unified with islanded resilience goals

This work improves microgrid control algorithms developed in (Nelson and Johnson, 2020) by incorporating islanded resilience goals within the grid-connected economic dispatch shown in Eq. (3). Weighting factors were added in the objective function to prioritize the dispatch of energy assets where ω_{grid}, ω_{gen}, and ω_{SOC} are the factors for utility import, generator fuel consumption, and battery SOC, respectively. The sum of the three weighting factors equals 1, and factors that have higher values result in decreased utilization of that asset. The effect of weighting factor selection is explored by sensitivity analysis to identify which combination of weights will enhance islanded resilience with no or negligible effect on grid-connected economics. Multi-objective optimization is not used here in order to directly preserve the concepts and metrics of grid-connected economics and islanded resilience.

$$J := \sum_{t=0}^{T_h} \omega_{grid} \left[\left(\sum_{\forall gen} \left(C_{gen}^{fuel} \times P_{gen,t} \times \eta_{gen} \right) + \sum_{\forall bat} \left(\left(C_{bat}^{OM,v} \times P_{bat,t}^{d} \right) + \left(C_{bat}^{OM,v} \times P_{bat,t}^{c} \right) \right) + \left(C_{grid,t}^{b} \times P_{grid,t}^{b} - C_{grid,t}^{s} \times P_{grid,t}^{s} \right) \right) \times \tau + \frac{T_h}{T_{bp}} \sum_{n=1}^{N_{TOU}} C_{grid,n}^{dem} \times {P_{grid,n}}^{max} + \left(\omega_{gen} \sum_{\forall gen} \left(P_{gen,t} \times \eta_{gen} \right) - \omega_{SOC} \sum_{\forall bat} \left(\frac{P_{bat}^{d,max}}{{E_{bat}}^{max}} \times E_{bat,t} \right) \right) \right] \quad (3)$$

3 Evaluation metrics

Microgrid survivability is a quantitative metric to describe the probability that a microgrid's critical load will be served. The following formulation uses statistical analysis and Markov Chains in (Nelson et al., 2020) with extensions to account for solar PV reliability. Matrices represent potential operating states of microgrid assets (generators, batteries, solar PV arrays) and reflect probabilities of the microgrid configuration to transition to a possible future operating state. From these probabilities, additional matrices are calculated to represent the ability to serve 100% of the critical load during the outage.

The state vector (size [$N\times$ 1]), expresses probabilities of each combination of microgrid assets being able to serve the critical load. The state vector length calculation, shown by Eq. (4), represents the total possible combinations of DERs. Microgrid survivability in the first time step of the islanded time horizon is found by the binomial distribution in Eq. 5 to model the probability of starting the islanding event with each possible combination of DERs. In this probability function, the statistical availability of each DER is considered where α_{gen}, α_{bat}, and α_{sol} are the percent availabilities of generators, batteries, and solar arrays, respectively, based on up-time and failure-to-start rates (Nelson et al., 2020; Ericson, 2019; Mrowca, 2011; EOS, 2023b). The previous work described in (Nelson et al., 2020) calculates microgrid survivability with an assumption that solar PV generators are 100% reliable (i.e., $\lambda_{sol}= 0$ and $\alpha_{sol}= 1$). This assumption neglects solar PV outages from inverter failures, ground faults, broken fuses and breakers (Abunima and Teh, 2020; Colli, 2015; Golnas, 2012), or physical failures due to mechanical load or extreme weather such as heat or hail (Skoczek et al., 2008). Here, this assumption is adapted to more accurately reflect solar PV operation. The total numbers of diesel generators, battery stacks, and solar arrays are reflected by N_{gen}, N_{bat}, and N_{sol}, respectively. The numbers of generators, battery stacks, and solar arrays available in each combination of operating states is reflected as g, b, and s, respectively.

$$N = \left(N_{gen} + 1 \right) \times \left(N_{bat} + 1 \right) \times \left(N_{sol} + 1 \right) - 1 \quad (4)$$

10.3389/fenrg.2023.1257050

$$p(0,g,b,s) = \left(\binom{N_{gen}}{g} \times \left(1-\alpha_{gen}\right)^{g} \times \left(\alpha_{gen}\right)^{N_{gen}-g}\right) \times \left(\binom{N_{bat}}{b} \times (1-\alpha_{bat})^{b} \times (\alpha_{bat})^{N_{bat}-b}\right) \times \left(\binom{N_{sol}}{s} \times (1-\alpha_{sol})^{s} \times (\alpha_{sol})^{N_{sol}-s}\right) \quad (5)$$

A transition matrix, $[T]$, can then be calculated to represent the probability of the microgrid to change from a current operating state to a potential future state with all possible combinations of DER assets, and reflects if the number of available DERs changes due to probabilistic failure. Each index of the transition matrix represents the probability of the current system's operating state to change to another operating state by accounting for the probability that any asset will fail over that time period. This probability calculation is shown in Eq. (6) where g, b, and s are the number of generators, battery stacks, and solar PV arrays, respectively, in the "current" operating state, with variables g', b', and s' as the number of assets in the "next" operating state, and λ_{gen}, λ_{bat}, and λ_{sol} representing the failure rates of DERs with units of $\frac{\#\text{ of failures}}{\text{hour}}$. The time step hourly fraction, τ, accounts for the simulation time resolution, for example, $\tau = 1$ represents hourly time steps, $\tau = 0.5$ represents 30-min intervals, and $\tau = 0.25$ represents 15-min intervals. Note that if a microgrid does not contain a certain type of asset (e.g., $N^{bat} = 0$), the corresponding term in the probability function will be set equal to one so that term does not influence the remaining parts of the equation set.

$$p(g,g',b,b',s,s') = \left(\binom{g}{g'} \times \left(1-\left(\lambda_{gen}\times\tau\right)\right)^{g} \times \left(\lambda_{gen}\times\tau\right)^{g-g'}\right) \times \left(\binom{b}{b'} \times (1-(\lambda_{bat}\times\tau))^{b} \times (\lambda_{bat}\times\tau)^{b-b'}\right) \times \left(\binom{s}{s'} \times (1-(\lambda_{sol}\times\tau))^{s} \times (\lambda_{sol}\times\tau)^{s-s'}\right) \quad (6)$$

Columns of the transition matrix represent all possible combinations of assets in the "current" operating state and the rows contain combinations of assets for possible "future" operating states. As a result, the transition matrix is an upper triangular matrix with size $[N \times N]$ due to the assumption that assets are not added to the microgrid during the simulation period. Eq. (7) describes the transition matrix and the dependency of each index term in relation to Eq. (6).

$$[T] = \begin{bmatrix} 1 & p(1,0,0,0,0,0) & \dots & p\left(N_{gen},0,N_{bat},0,N_{sol},0\right) \\ 0 & p(1,1,0,0,0,0) & \dots & p\left(N_{gen},1,N_{bat},0,N_{sol},0\right) \\ \vdots & \vdots & \ddots & \vdots \\ 0 & \dots & 0 & p\left(N_{gen},N_{gen},N_{bat},N_{bat},N_{sol},N_{sol}\right) \end{bmatrix} \quad (7)$$

Eq. (8) shows the calculation for microgrid power generation at time, t, demonstrating a worst-case scenario approach by only considering the minimum output of assets based on operational and technical limitations. Generator contribution to total generation capacity is shown by the onsite fuel availability in gal, F_t^{av}, fuel conversion rate of the generators in gal/kWh, ρ_{gen}, and power capacity of all microgrid generators, P_{gen}. Battery contributions are reflected by the energy contained in all battery stacks, E_{bat}, minimum energy storage capacity of a battery stack, $E_{bat}{}^{min}$, the efficiency of a battery stack, η_{bat}, and the maximum discharge of a battery stack, $P_{bat}^{d,max}$. Solar PV contribution is reflected by the total output of solar units, P_{sol}. Eq. (9) expresses the probability of microgrid survival with g, b, and s available generators, battery stacks, and solar arrays at time, t, and applies for all state vectors in the time horizon, with the initial state vector using the probability as shown in Eq. (6) that uses DER failure-to-start rates. Those calculations following the initial state are based on the previous operating states and operating failure rates. The microgrid state vector of an islanding event beginning at time t can be calculated by performing matrix multiplication of the transition matrix with the microgrid state vector from the previous time step, as shown in Eq. (10). Eq. (11) expresses microgrid survivability in each time step by summing entries in the state vector at each time step.

$$P_t^{tot} = g \times \min\left(\frac{\frac{F_t^{av}}{g}}{\rho_{gen}\times\tau}, P_{gen}\right) + b \times \min\left(\frac{E_{bat} - E_{bat}{}^{min}}{\tau} \times \eta_{bat}, P_{bat}^{d,max}\right) + (s \times P_{sol}) \quad (8)$$

$$s_h(t,g,b,s) = \begin{cases} 0, P_t^{tot}(t) < P_t^{crit} \\ p(t,g,b,s), P_t^{tot}(t) \geq P_t^{crit} \end{cases} \quad (9)$$

$$[S_{h,t+1}] = \begin{bmatrix} s_h(t+1,0,0,0) \\ s_h(t+1,1,0,0) \\ \vdots \\ s_h\left(t+1,N_{gen},N_{bat},N_{sol}\right) \end{bmatrix} = \begin{bmatrix} 1\,p(1,0,0,0,0,0)\dots & p\left(N_{gen},0,N_{bat},0,N_{sol},0\right) \\ 0\,p(1,1,0,0,0,0)\dots & p\left(N_{gen},1,N_{bat},0,N_{sol},0\right) \\ \vdots \quad \vdots \quad \ddots & \vdots \\ 0 \quad \dots \quad 0 & p\left(N_{gen},N_{gen},N_{bat},N_{bat},N_{sol},N_{sol}\right) \end{bmatrix} \begin{bmatrix} s_h(t,0,0,0) \\ s_h(t,1,0,0) \\ \vdots \\ s_h\left(t,N_{gen},N_{bat},N_{sol}\right) \end{bmatrix} \quad (10)$$

$$S_h(t) = \sum_{\forall g}^{N_{gen}} \sum_{\forall b}^{N_{bat}} \sum_{\forall s}^{N_{sol}} s_h(t,g,b,s) \quad (11)$$

Four technical metrics, three economic metrics, and one environmental metric are used to evaluate the performance of microgrid control algorithms. Technical metrics include survivability, autonomy, fuel consumption, and unserved energy. Economic metrics include microgrid O&M cost, revenue from energy sales, and net operational cost. The environmental metric is carbon intensity. Eq. (12) expresses the average probability of surviving a microgrid islanding event over a simulation where Q is the distribution of outage starts and q_t is the probability of an islanding event starting in time step t of a simulation. A uniform distribution is assumed for q_t to indicate an islanding event has equal probability to start at any time step in the simulation time period, T_{sim}.

TABLE 1 Operational characteristics of battery storage (EOS, 2023a).

Round-trip efficiency (%)	Self-discharge (fraction of capacity lost per hour)	C-rate	Min/Max SOC (kWh)	Unit capacity (kWh)	Lifetime (cycles)	Up-time (%/year)
75	0.01	C/4	0/600	600	5,000+	98

TABLE 2 Asset financial data for optimal sizing and selection for hybrid microgrid.

Technology	Capital cost	Annual O&M cost	Fuel	Variable O&M
Generator	$750/kW (ESTCP, 2019)	$9.33/kW/year (ESTCP, 2019)	$2.97/gal	-
Solar PV	$2,100/kW (Fu et al., 2018)	$17.04/kW/year (Fu et al., 2018)	-	-
Battery	$436/kWh (EOS, 2023a)	$3.96/kWh/year (EOS, 2023a)	-	$0.0436/kWh (ESTCP, 2019)

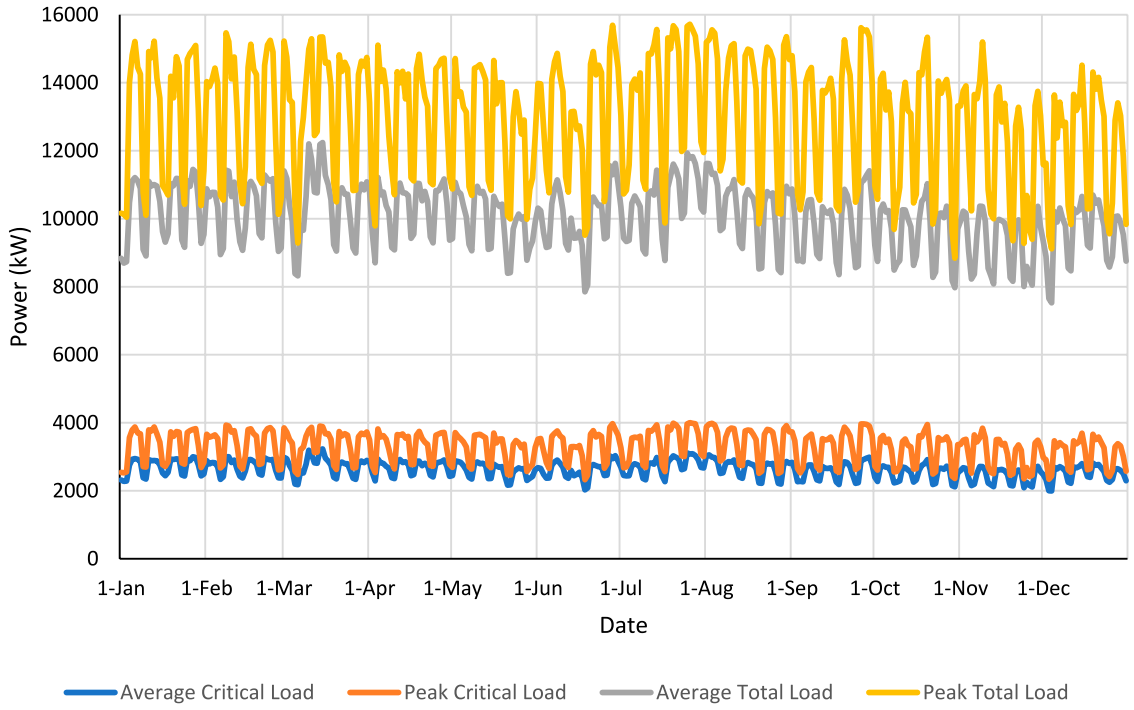

FIGURE 2
Daily critical load and total load.

$$\overline{S_h}(t,Q) = \sum_{t=0}^{T_{sim}} q_t S_h(t) \tag{12}$$

Eq. (13) represents autonomy by summing the slack binary variable, B_t^{slack}, across each time step in the time horizon to measure the time where critical load is fully met. Autonomy, A, represents the duration of time that 100% of the critical load can be served during an islanding event.

$$A = \sum_{t=0}^{T_h} B_t^{slack} \times \tau \text{ where } \begin{cases} B_t^{slack} = 1, P_t^{slack} = 0 \\ B_t^{slack} = 0, P_t^{slack} \neq 0 \end{cases} \tag{13}$$

Eq. (14) shows the calculation for total fuel consumption during an islanding event. Fuel consumption is the product of the generator fuel consumption rate with the generator power output and time step hourly fraction.

$$F_{gen}^{tot} = \sum_{t=0}^{T_h} \left[\sum_{g=0}^{N_{gen}} \rho_{gen} \times P_{gen,t} \times \tau \right] \tag{14}$$

Eq. (15) shows the calculation for unserved energy. The total unserved energy during an islanding event is found by summing the curtailed load for the duration of the islanding event.

$$E_{unserved} = \sum_{t=0}^{T_h} P_t^{slack} \times \tau \tag{15}$$

Eq. (16) expresses the microgrid O&M cost for all DER assets. As discussed in Section 2.1, the sources of microgrid O&M can be

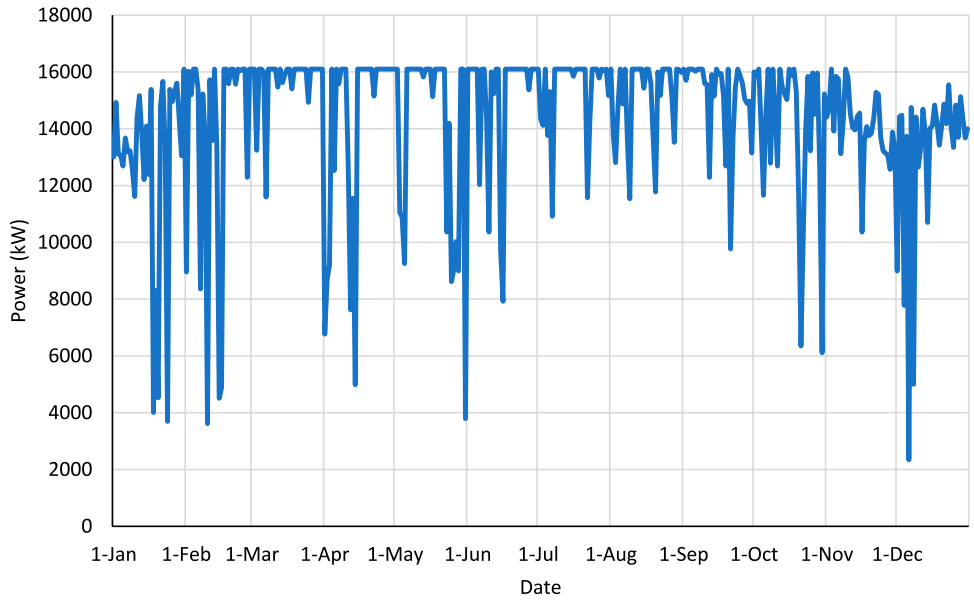

FIGURE 3
Daily peak solar PV output.

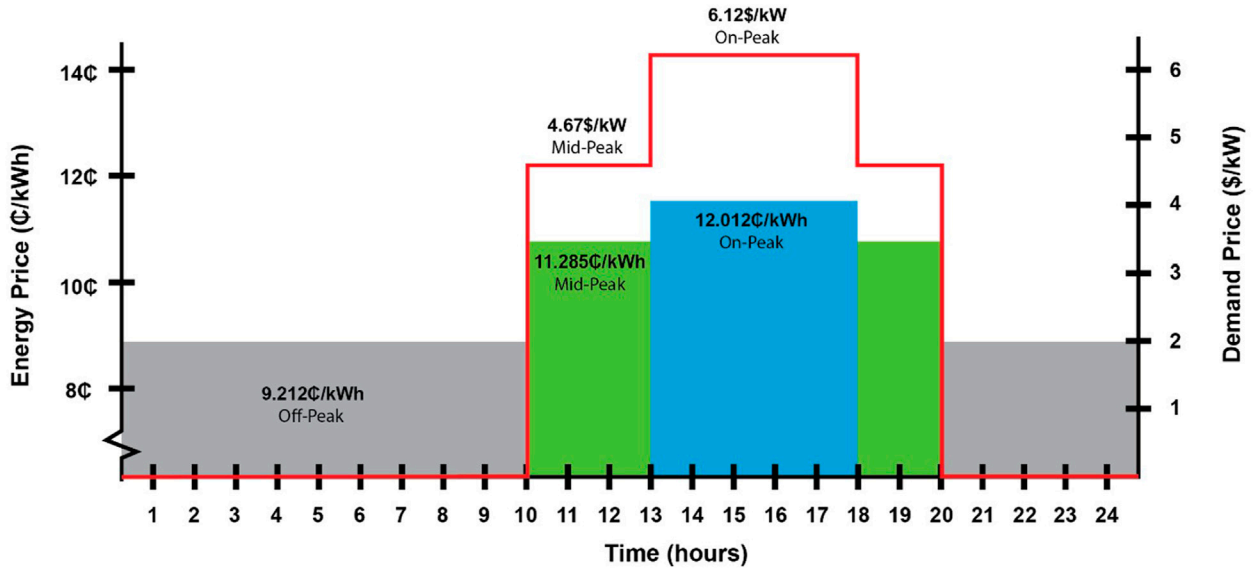

FIGURE 4
Utility rate structure for Summer.

influenced by contractual agreements for O&M. In this work, microgrid O&M cost includes fuel use by generators and battery degradation. In some use cases, microgrid O&M can also include fixed and variable generator O&M and fixed and variable solar PV O&M. Eq. (17) expresses microgrid revenue from energy sales to the utility. Energy sales use a net metering assumption where the compensation price is set equal to the purchase price of energy, and if energy sales exceed energy purchases in a billing period, market wholesale rates are used to credit the microgrid for energy sales. Eq. (18) expresses net operating costs, which include dispatch from DERs and utility import energy and demand costs. These costs a reduced by revenue from energy sales.

$$C^{OM} = \sum_{t=0}^{T_{sim}} \left[\sum_{\forall gen} \left(C_{gen}^{fuel} \times P_{gen,t} \times \eta_{gen} \right) + \sum_{\forall bat} \left(\left(C_{bat}^{OM,v} \times P_{bat,t}^{d} \right) + \left(C_{bat}^{OM,v} \times P_{bat,t}^{c} \right) \right) \right] \times \tau \tag{16}$$

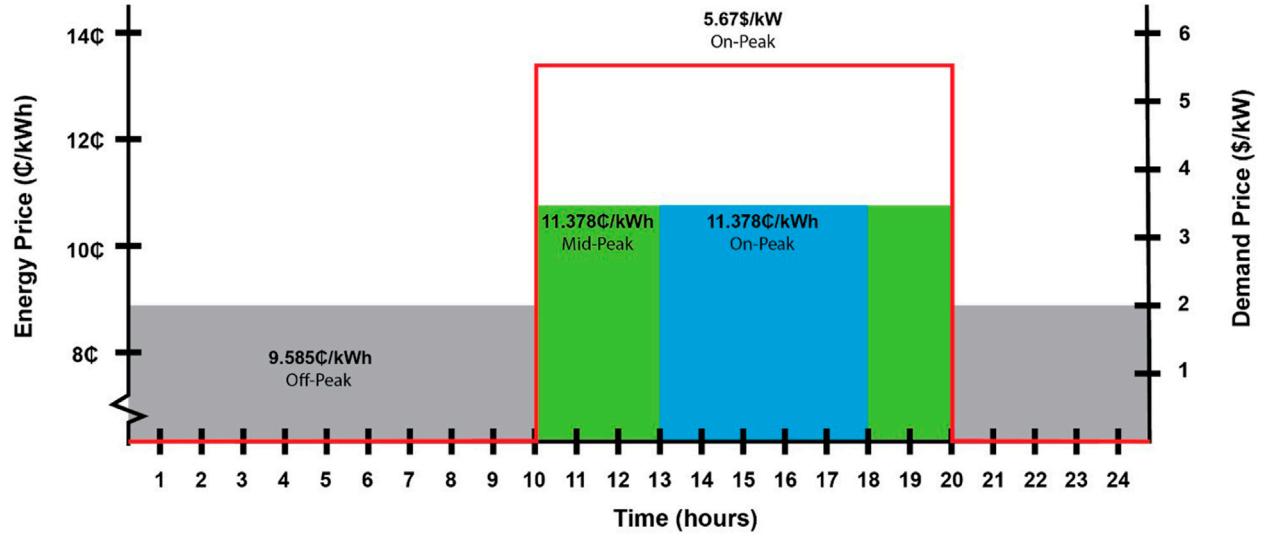

FIGURE 5
Utility rate structure for Winter.

TABLE 3 Optimal sizing of microgrid assets.

Generator units	Total generator capacity (kW)	Solar PV area (m^2)	Total solar PV capacity (kW)	Battery units	Total battery storage capacity (kWh)
3	2,250	109,862	16,479	23	13,800

TABLE 4 Summary of sensitivity analyses.

ω_{grid}	ω_{gen}	ω_{SOC}	ω_{gen}	ω_{SOC}	ω_{gen}	ω_{SOC}	ω_{gen}	ω_{SOC}	ω_{gen}	ω_{SOC}	ω_{gen}	ω_{SOC}
0	0	1.0	0.2	0.8	0.4	0.6	0.6	0.4	0.8	0.2	1.0	0
0.2	0	0.8	0.2	0.6	0.4	0.4	0.6	0.2	0.8	0	-	-
0.4	0	0.6	0.2	0.4	0.4	0.2	0.6	0	-	-	-	-
0.6	0	0.4	0.2	0.2	0.4	0	-	-	-	-	-	-
0.8	0	0.2	0.2	0	-	-	-	-	-	-	-	-
1.0	0	0	-	-	-	-	-	-	-	-	-	-

$$C^s_{grid} = \sum_{t=0}^{T_{sim}} \left(C^s_{grid,t} \times P^s_{grid,t} \right) \times \tau \tag{17}$$

$$C^{net} = C^{OM} + \left(\sum_{t=0}^{T_{sim}} \left(C^b_{grid,t} \times P^b_{grid,t} \right) \times \tau + \frac{T_h}{T_{bp}} \sum_{n=1}^{N_{TOU}} \left(C^{dem}_{grid,n} \times {P_{grid,n}}^{max} \right) \right) - C^s_{grid} \tag{18}$$

Eq. (19) shows the calculation of total carbon intensity, β^{tot}, associated with energy consumption from utility import and local power generation from diesel generators. Both terms use emissions factors to represent the rate at which carbon is emitted per unit of energy generated by each source. The utility import emissions factor uses publicly available data from the California Independent System Operator (CAISO). Monthly emissions data (California ISO, 2023) and utility energy supply (Blanke, 2019) provide the average annual emissions factor, ϵ_{grid}. The generator emissions factor, ϵ_{gen}, uses the rate of carbon emissions from diesel fuel (The Climate Registry, 2022) and generator efficiency to equate carbon emissions from diesel generators.

$$\beta^{tot} = \sum_{t=0}^{T_{sim}} \left(\left(P^b_{grid,t} \times \epsilon_{grid} \right) + \sum_{\forall gen} \left(P_{gen,t} \times \epsilon_{gen} \right) \right) \times \tau \tag{19}$$

4 Microgrid case study

4.1 Microgrid specification data

A military installation distribution system is used as the microgrid case study given increasing interest from the United States Office of

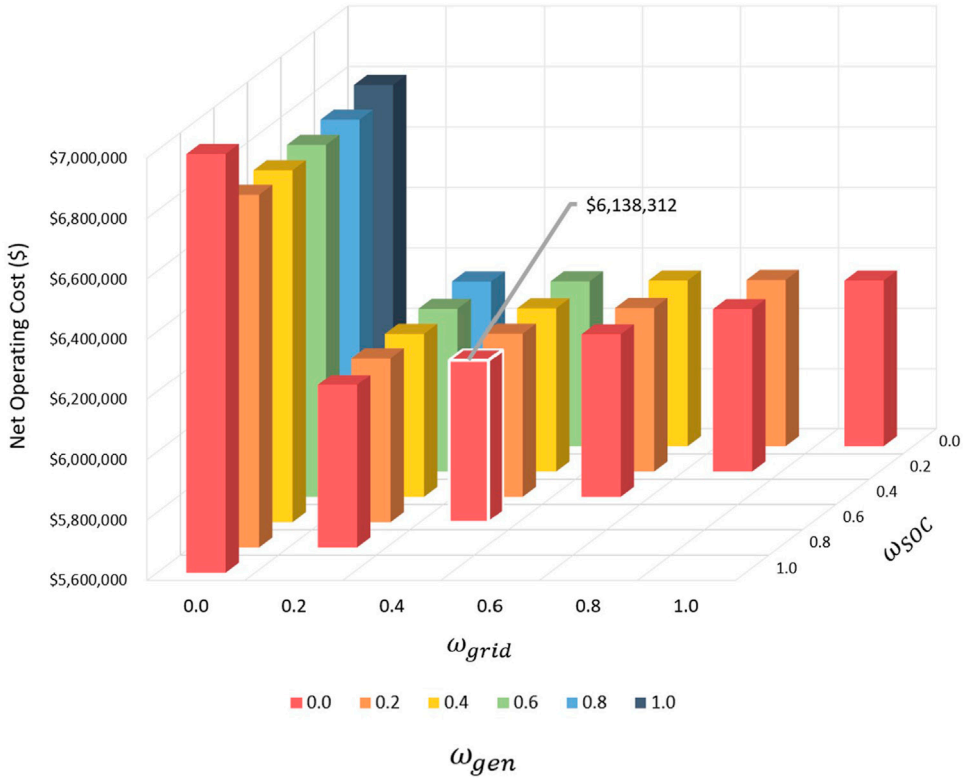

FIGURE 6
Sensitivity analysis showing annual economic results. The case with the lowest net operating cost is outlined in white.

the Secretary of Defense (OSD) to maintain resilience and load-serving capability during utility islanding events (Johnson, 2022). Sensitive information is anonymized.

4.2 Microgrid assets

Potential microgrid assets included diesel generators, battery storage, and solar PV. A Cummins 750 kW diesel generator was used with an assumed constant fuel conversion rate, ρ_{gen}, of 0.0727 gal/kWh calculated from a linear regression (R^2= 0.9962) from manufacturer data (Power, 2007). The lower-heating value, LHV_{fuel}, of diesel fuel is 37.65 kWh/gal (ESSOM, 2016). Onsite fuel storage, F_0^{av}, is assumed to be 25,000 gallons (ESTCP, 2019). Per contractual agreement, fuel is resupplied on the first day of each month, and any fuel used for grid-connected operation reduces fuel reserves available at the start of an islanding event until the next resupply occurs. Metrics for up-time, failure to start (FTS), and mean time to failure (MTTF) rates were taken to be 99.9%, 0.02%, and 1700 h, respectively (ESTCP, 2019). Battery storage operating characteristics are shown in Table 1 for an EOS zinc aqueous technology (EOS, 2023a). The starting battery SOC at the beginning of simulations, E_{bat}^{init}, is assumed to be 50% to reflect regular use of the battery for energy shifting and peak shaving, rather than being simply used for backup power.

Financial data for capital cost, O&M cost, and fuel are provided in Table 2 for all asset types (ESTCP, 2019). Asset capital cost and annual O&M cost are included in the microgrid sizing study because they affect project payback period and sizing economics, but are not included in the dispatch study and main results demonstrated in this work because they do not affect dispatch economics. An average annual inflation rate of 2.2% and nominal investment discount rate of 6.0% were assumed for a 20-year investment period (ESTCP, 2019). Tax incentives include the U.S. federal investment tax credit (ITC) that permits 30% credit towards the developer's or operator's taxes, and the Modified Accelerated Cost Recovery System (MACRS) of 5 years to accelerate tax deductions for renewable asset depreciation (Sherlock, 2018). These incentives were applied to the capital costs of solar PV and battery storage. To be eligible for the ITC, battery charging was restricted to renewable sources of generation when grid-connected.

4.3 Military installation load profile and solar production

The daily peak and daily average values are shown in Figure 2 for the critical load, $P_{l,t}^{crit}$, () and total load, $P_{l,t}^{crit} + P_{l,t}^{ctrl}$. Microgrid critical load (load served during islanded operation) is 26.7% of total installation load. During microgrid islanding, non-critical loads are isolated from microgrid generation assets via manual switchgear operations by installation personnel. Modeling of other types of curtailable loads is outside the scope of this work. Figure 3 shows the daily peak solar PV generation, $P_{sol,t}^{for}$, using the cost-optimal solar PV array capacity, with AC output simulated in National Renewable Energy Laboratory's (NREL) SAM tool (ESTCP, 2019) using local solar irradiance weather data, panel performance and orientation, and inverter and balance of system losses.

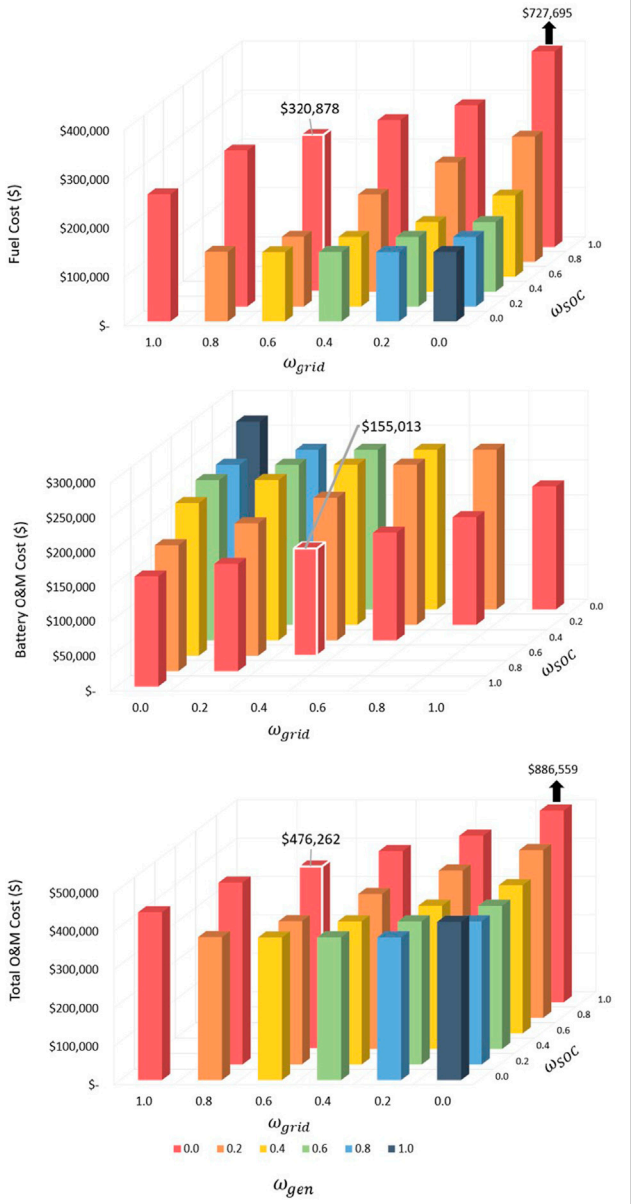

FIGURE 7
Sensitivity analysis of O&M costs. Two cases with values above the z-axis are indicated with black arrow and text, which are truncated for better visualization of the graph topology. The case with the lowest net cost is outlined in white.

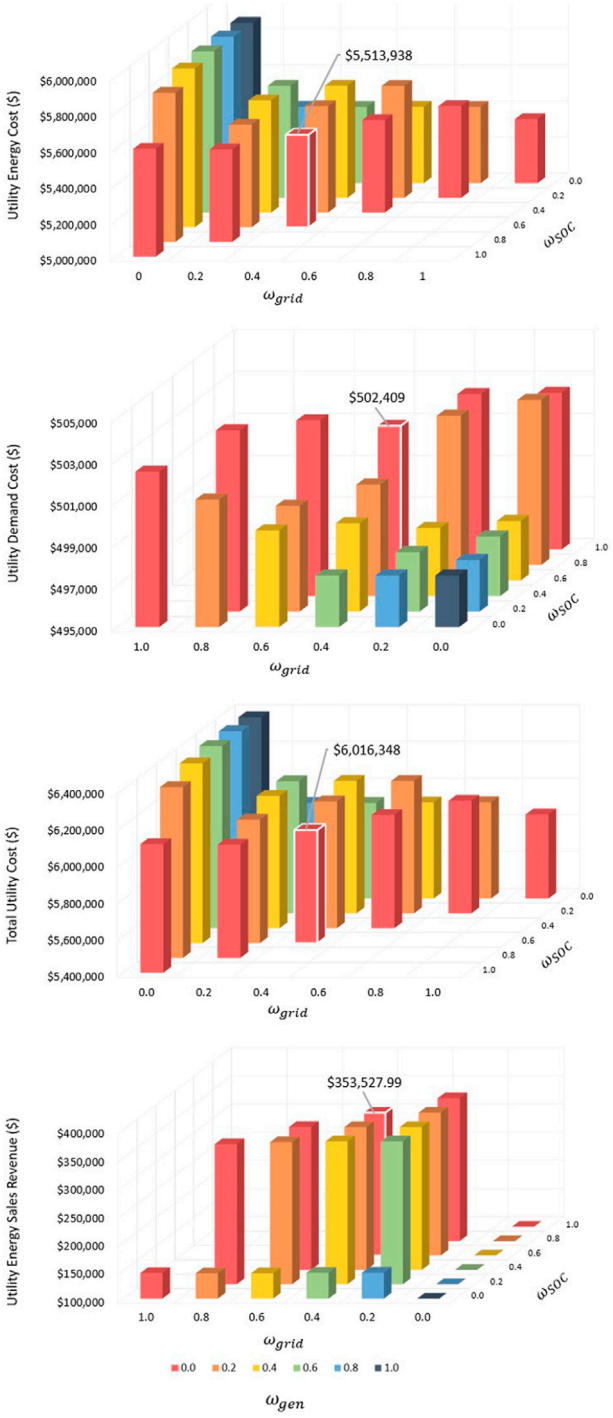

FIGURE 8
Sensitivity analysis of utility cost components and energy sales revenue. The case with the lowest net cost is outlined in white.

4.4 Utility costs

Energy costs differ for summer (June through September) and winter (October through May). Figures 4, 5 show the TOU rate structure for energy, $C^{b}_{grid,t}$, and demand charges, $C^{dem}_{grid,n}$, for summer and winter seasons, respectively. This use case operates on a net metering assumption, so all energy sales are credited back on the utility bill at the same rate as the purchase cost. The utility wholesale rate is applied to bill credits ($C^{s}_{grid,t} = 0.02839$/kWh) in which energy sales exceed the energy purchased.

4.5 Optimal microgrid portfolio

Asset sizes were selected by optimizing for lowest cost grid-connected operations using XENDEE (Stadler and Naslé, 2019; Pecenak et al., 2019). XENDEE is a cloud computing software that jointly performs techno-economic optimization and power systems analysis. XENDEE's economic optimization tool selects,

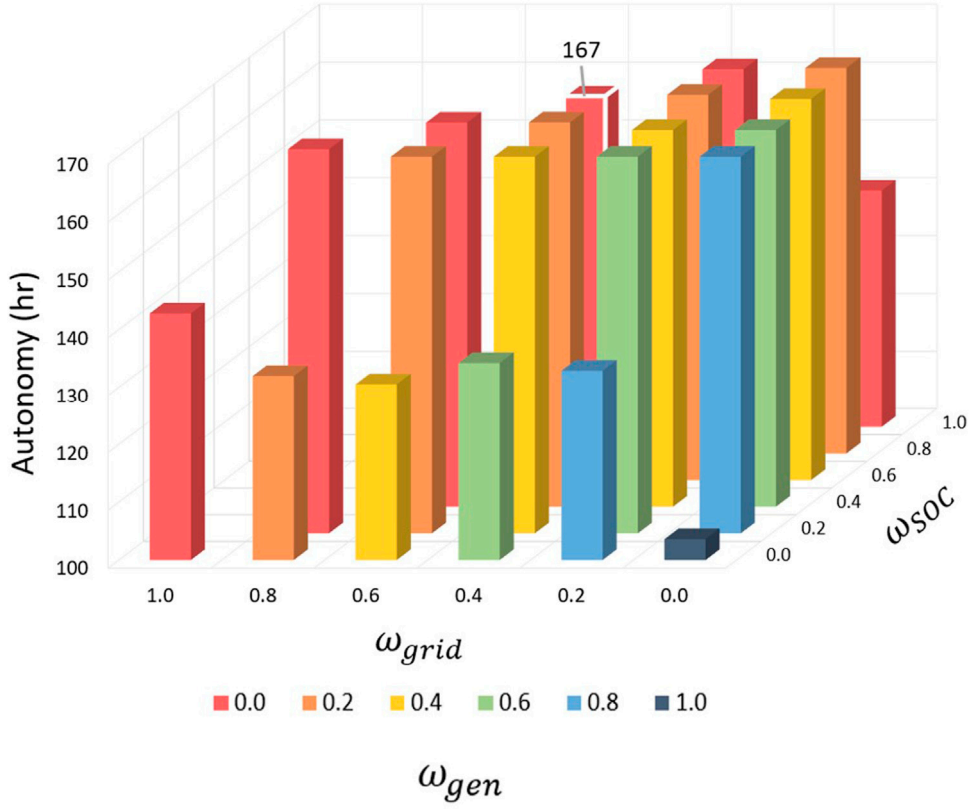

FIGURE 9
Sensitivity analysis islanded autonomy. The case with the lowest net cost is outlined in white.

sizes, places, and dispatches energy assets within a microgrid portfolio using MILP. XENDEE minimizes total annual costs of providing energy services to a customer considering system energy demand, regulatory requirements, and energy procurement costs, including monthly fixed utility costs, volumetric electricity purchases, demand charges, annualized technology investment costs, and technology O&M costs during grid-connected and islanding operations. The optimization formulation accounts for technical operating constraints of the considered technologies (e.g., charging/discharging limits of battery stacks) and environmental conditions (e.g., solar irradiance) that influence the capacity of onsite renewable generation. Grid-connected economic dispatch in XENDEE was completed using the local utility tariff that consists of monthly fixed charges, distribution charges, on-peak energy charges, mid-peak energy charges, off-peak energy charges, monthly peak demand charges, and taxes.

XENDEE yielded the cost-optimal asset types and capacities listed in Table 3. This microgrid portfolio is used in remaining sections to exercise the proposed unified dispatch algorithm for grid-connected economic operation and islanded resilience operation.

5 Results

Sensitivity analysis was used to evaluate the effect of weighting factors for the grid-connected objective function (Eq. (3)). Each weighting factor was varied from zero to one in steps of 0.2, keeping the summation of the three factors (ω_{grid},ω_{gen},ω_{SOC}) equal to one. Weighting factors are summed to one so each term in the objective can be prioritized as parts of a whole (fraction of 100%). The step-size of 0,2 is selected to limit the number of simulations to be conducted, allowing for clarity and manageability of results. The resulting 21 combinations of weighting factors shown in Table 4 omit repeat combinations. For each sensitivity combination, an annual simulation was completed of grid-connected dispatch to equate economic results, fuel use, battery SOC profile, and carbon intensity data. The resulting fuel and battery SOC capacities for each time step of the year were then used as starting states for islanded dispatch, thereby simulating an unexpected grid outage for every hour of the year. Sections 5.1–5.3 demonstrate and analyze results for grid-connected operational costs, islanded resilience, and environmental impact, respectively. Section 5.4 summarizes the selection of optimal weighting factors for microgrid control to jointly prioritize goals for grid-connected and islanded operation.

5.1 Grid-connected operation and economics

Figure 6 shows the net operational cost for each combination in the sentivity analysis comprised of grid energy costs, grid demand costs, microgrid O&M costs, fuel costs, and grid energy sales. Inclusion of the grid weighting factor (i.e., $\omega_{grid} > 0$) in the unified

dispatch formulation results in an average reduction of $665,200 in net operating cost across sensitivity combinations where $\omega_{grid} > 0$. Optimizations using any non-zero grid weighting value showed minimal variation in net operating cost (0.22%), indicating that selection of weighting factors above $\omega_{grid} = 0$ have similar economic savings. For this case study, the lowest net operating cost occurs when $\omega_{grid} = 0.2$, $\omega_{SOC} = 0.8$, and $\omega_{gen} = 0$ by delivering reductions in utility costs and battery O&M costs that offset higher diesel fuel costs, relative to other combinations of weighting factors. Figure 7 graphs the contributing factors to net operating cost including the annual fuel cost, battery O&M cost, and total O&M cost for each sensitvity combination. The trends across the fuel and battery O&M graphs show there is an inverse relationship as the priortization of onsite fuel (ω_{gen}) changes: When ω_{gen} ranges from zero to one (red to blue bars in Figure 7), the cost of fuel consumed during grid-connected operation decreases by $586,066 due to increased weighting of fuel consumption in the objective funciton; Subsequently, as ω_{gen} ranges from zero to one, battery O&M cost increases by $115,983 due to batteries being dispatched to replace diesel generation and preserve onsite fuel. The total O&M plot is relatively flat across simulations where $\omega_{gen} > 0$ due to the trade-off in dispatch of energy assets (and associated O&M costs) as weighting factors shift priorities in the objective function. This indicates that the selection of weighting factors has little impact on total O&M cost even though larger changes are observed in the individual contributors to total cost. Figure 8 illustrates changes to utility energy costs, demand costs, and total utility costs for all combinations of sensitvity weighting factors. Energy costs are the largest contributor to total utility cost (>90%) with the reminder comprised of demand costs. Revenue was also calculated, and the revenue from energy sales contribute is larger when ω_{gen} and ω_{SOC} are greater than greater than zero. Revenues from energy sales contribute to the flattening shape of net operating cost in Figure 6, making the choice of the grid weighting factor insignificant for all positive non-zero values.

5.2 Islanded resilience

Figures 9, 10 show the average islanded microgrid autonomy and average unserved energy during islanded operations, respectively, computed across simulations of a 168-h duration grid outage starting at every time step in a year. In Figure 9, cases where $\omega_{SOC} = 0$ ($\omega_{gen} > 0$ and $\omega_{grid} > 0$) demonstrate the worst performing autonomy across the sensitivity analysis, and in cases when $\omega_{gen} = 0$ ($\omega_{SOC} > 0$ and $\omega_{grid} > 0$) or when all weights are >0 the autonomy is improved by an average of 22.4% and 28.1%, respectively. This demonstrates that when resilience terms are included in the grid-connected objective, unified dispatch preserves energy from DERs (i.e., battery storage and generator fuel) and improves ability to survive utility outages and power critical loads. Figure 10 shows that unserved energy (curtailed power) is significantly higher when either ω_{SOC} or ω_{gen} are zero because batteries and generators are more freely

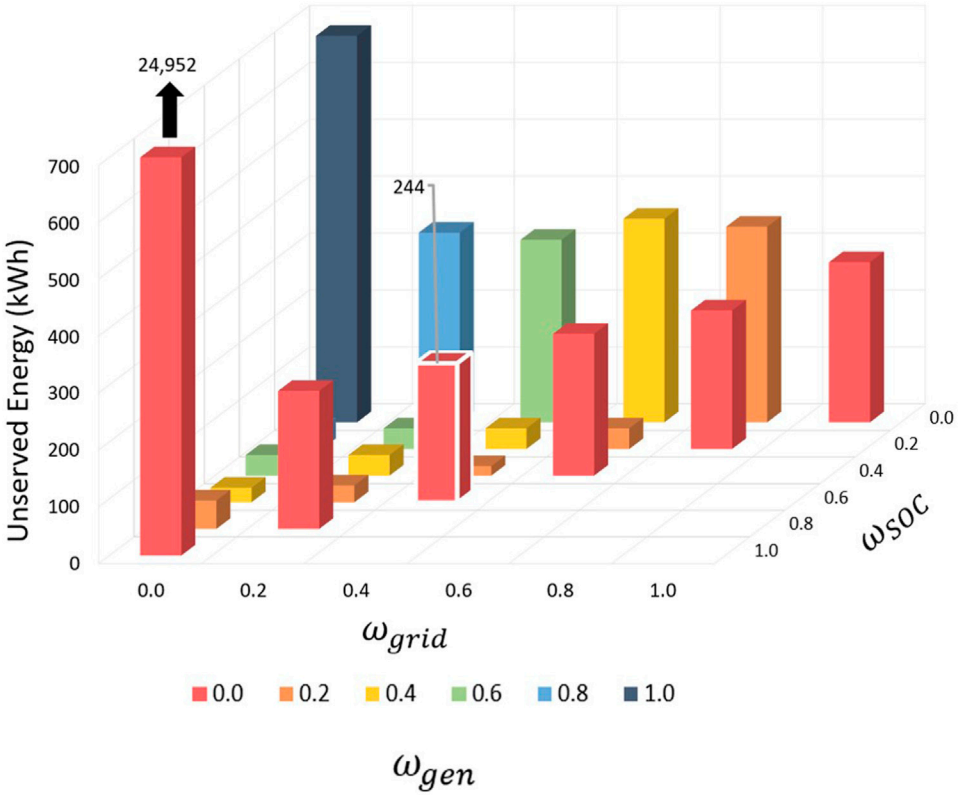

FIGURE 10
Sensitivity analysis unserved energy during islanded operation. One case with unserved energy above the range of the *z*-axis is shown by a black arrow and text. The case with the lowest net cost is outlined in white.

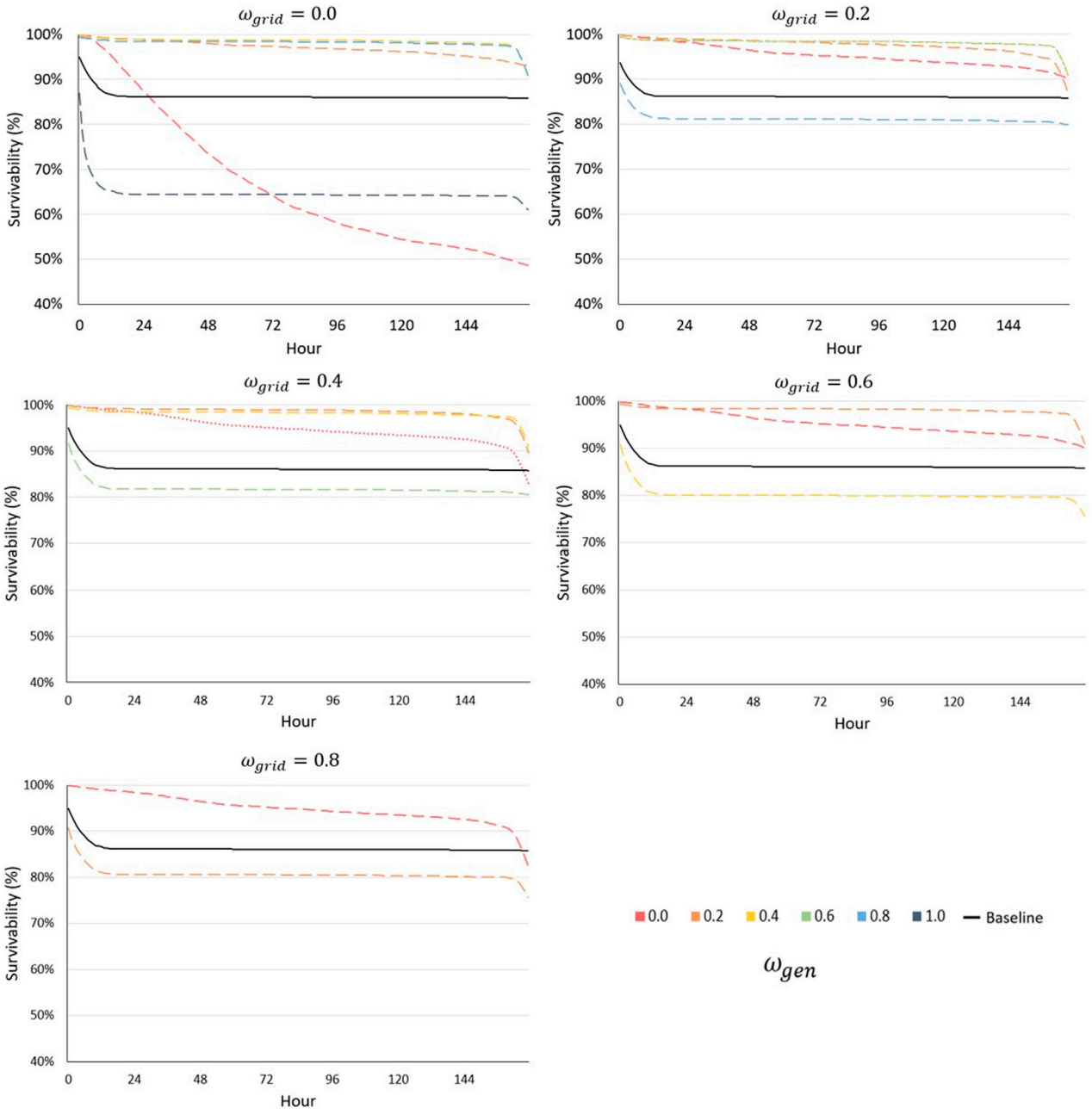

FIGURE 11
Sensitivity analysis islanded survivability. The case with the lowest net cost is indicated by the dotted-line.

dispatched to meet the grid-connected load for cost reduction purposes, resulting in less stored energy and onsite fuel stored at the start of an islanding event. Autonomy worsens further when ω_{SOC}= 0 and ω_{grid}= 0 because generator dispatch becomes the only contribution to the grid-connected objective, which does preserve fuel but results in greater dispatch of batteries and less stored energy to meet power needs of the critical load across long time periods. Similarly, when ω_{SOC}= 1 and other terms are zero, the generator is heavily dispatched and fuel reserves are significantly depleted, leading to greater amounts of load shedding during an islanding event. Figure 10 shows an average reduction of 98.7% in unserved energy when both ω_{gen} and ω_{SOC} have values greater than zero, resulting from the increased availability of onsite fuel and battery storage at the start of the islanding event. Adding these resilience terms to a traditional economic optimization formulation creates solutions that result in higher availability during islanded operations. Minimal variation is observed in both autonomy (0.91%) and unserved energy (1.32%) when both ω_{gen} and ω_{SOC} are included in the objective function.

Figure 11 shows the average survivability for islanded operation across all sensitivity cases. Survivability decreases over time with respect to the increasing statistical likelihood for assets to fail and diesel fuel reserves to become depleted. The optimization weight sensitivity cases are compared to the baseline in which ω_{grid} = 1, ω_{gen}= 0, and ω_{SOC} = 0

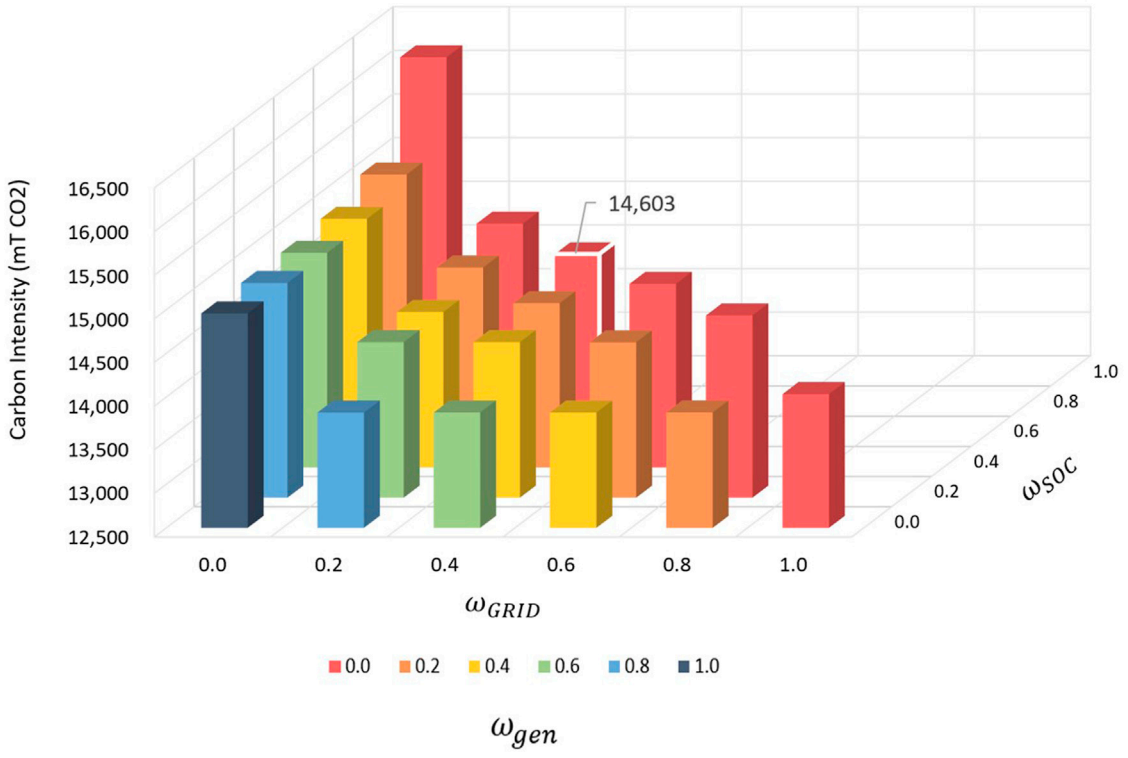

FIGURE 12
Sensitivity analysis carbon intensity results. The case with the lowest net cost is outlined in white.

TABLE 5 Summary of weighting factor combinations for illustrative cases.

ω_{grid}	ω_{gen}	ω_{SOC}	Net operating cost ($)	Autonomy (hr)	Unserved energy (kWh)	Ending survivability (%)	Carbon intensity (mT $C0_2$)
0.4	0.2	0.4	6,141,938	166.6	16.7	89.6	14,382
0.4	0.4	0.2	6,142,203	165.3	36.3	90.9	14,282
0.6	0.2	0.2	6,143,295	165.3	36.2	90.9	14,280

(i.e., no resilience considerations during grid-connected operation). Figure 11 shows that for each ω_{grid} plot, cases in which $\omega_{SOC} = 0$ deplete the battery and result in the lowest survivability, except in the case in which $\omega_{grid} = 0$, $\omega_{gen} = 0$, and $\omega_{SOC} = 1$ yields a lower survivability for longer outages as fuel reserves are depleted on average over the simulated year. Including the generator term and storage term in the objective function (setting both ω_{gen} and ω_{SOC} to non-zero values) always yields an improvement in survivability over the baseline case that only considered grid energy costs ($\omega_{grid} = 1$) in the grid-connected objective function. These results parallel those shown in Figure 10 and clearly illustrate that the set of sensitivity cases with all three weights set to positive non-zero values yield similarly favorable results for all three resilience metrics.

5.3 Environmental impacts

Figure 12 shows carbon intensity associated with each sensitivity case. Carbon intensity comprises emissions from utility power purchases and generator power output. Any excess solar exported to the utility is not counted as a credit to reduce carbon intensity. The utility import emission factor and diesel generator emmision factor are 0.241 $\frac{\text{mT CO}_2}{\text{MWh}}$ (California ISO, 2023; Blanke, 2019; 0.701 $\frac{\text{mT CO}_2}{\text{MWh}}$ The Climate Registry, 2022), respectively. The hybrid microgrid reduces carbon intensity by using solar PV at the time of production and storing excess solar PV generation to displace grid purchases and generator use. The variations in carbon intensity shown in Figure 12 are attributed to diesel generators being dispatched to minimze grid demand charges and preserve a high battery SOC. As ω_{gen} increases, generators are dispatched less frequently, resulting in an overall reduction of carbon intensity because the emissions factor for generators is higher than the emissions factor for grid imports. This behavior occurs regardless of the grid weighting factor. The worst carbon intensity is observed when both $\omega_{gen} = 0$ and $\omega_{grid} = 0$, matching the expected conceptual understanding that emissions will be highest when generator and grid terms are excluded from the cost-minimizing objective function with no penality against using those carbon-producing sources. As

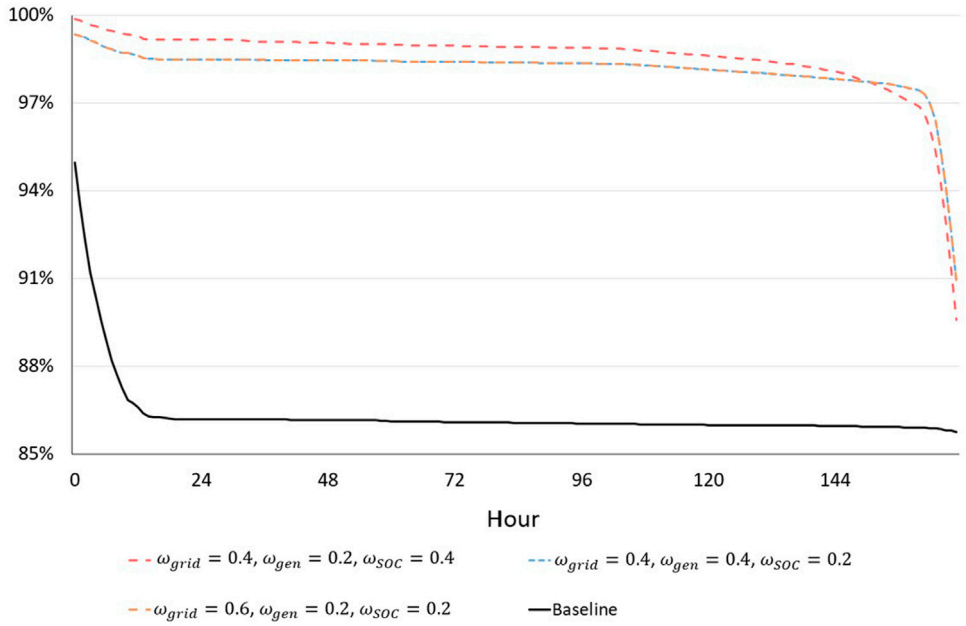

FIGURE 13
Survivability of weighting factor combinations selected to illustrate best case operations for combined grid-connected economics and islanded resilience.

TABLE 6 Summary of operational characteristics for optimal control parameters compared to baseline.

	ω_{grid}	ω_{gen}	ω_{SOC}	Net operating cost ($)	Autonomy (hr)	Unserved energy (kWh)	Ending surviability (%)	Carbon production (mT CO_2)
Baseline	1.0	0.0	0.0	6,150,293	142.8	281.2	85.7	14,032
Optimized	0.4	0.2	0.4	6,141,938	166.6	16.7	89.6	14,382
Percent Difference (%)				−0.1%	+16.7%	−94.1%	+3.9%	+2.5%

ω_{SOC} increases, stored energy in the battery bank is increasingly reserved for a potential unplanned islanding event, and this behavior deceases the frequency in which batteries are used to store excess solar PV and dispatch excess to serve loads, resulting in a higher use of carbon-producing sources. Results show that reductions in carbon intensity are best achieved for weighting factor combinations that prioritize ω_{grid} and ω_{gen} and set $\omega_{SOC} = 0$.

5.4 Optimal microgrid operations

Results in Table 5 summarize the subset of sensitivity cases that yielded similarly favorable results. For improved economics, any non-zero value for ω_{grid} produced minimal change in annual net operating cost relative to sensitivity cases with $\omega_{grid} = 0$ that were an average of 11% higher in cost. For improved islanded resilience, results showed that autonomy, unserved energy, and survivability improved with the selection of all three weighting factors to be non-zero, meaning that all three terms in the objective function were active. Results of the case $\omega_{grid} = 0.4$, $\omega_{gen} = 0.2$, and $\omega_{SOC} = 0.4$ in Figure 13 show a higher survivability over nearly all hours of a 168-h (7-day) outage, resulting from the optimization algorithm focus on preserving battery storage for the event of an outage. These results complement other results in Table 5. Carbon intensity is slightly higher and net operating cost slightly lower, relative to the other two cases in Table 5. Results shown in Table 6 compare this case to the baseline case in which $\omega_{grid} = 1$. Operational behavior arising from the objective function with all three terms shows an improvement in net operating cost, autonomy, unserved energy, and survivability, with a small increase in carbon intensity from increased use of the generator to reduce grid demand charges and maintain higher battery SOC.

6 Conclusion

This work developed a simulation environment and tertiary controls approach for microgrid economic dispatch and resilience dispatch for grid-connected and islanded operations, respectively. Results demonstrated that including resilience terms in the optimization formulation for grid-connected economic dispatch produced more favorable resilience results, and also yielded a modest improvement in economic results. Optimal selection of weighting factors used in the microgrid control strategy resulted

in islanding operational results with a 3.9% improvement in survivability, a 94.1% reduction in unserved energy, and a 16.7% improvement in autonomy, while also delivering a reduction in annual net costs of 0.1%, at the expense of a small increase in carbon intensity of 2.5% relative to the baseline case.

This approach is generalizable for use as a planning tool or during real-time operational control to reflect changing conditions where weighting factors can be selected and tuned to match microgrid goals relative to the situation (e.g., depleted fuel reserves, asset outage, estimated grid outage duration). It may also be beneficial to chose different weighting factors to consider operating conditions such as volitile fuel prices, such as those seen following the global COVID-19 pandemic or conflict in Ukraine (US Energy Information Administration, 2022), utility rate changes, and various types of technology O&M agreements. Microgrid performance during islanded conditions can be improved by tuning weighting factors that maximize battery SOC, and hence, improve the ability of the microgrid to meet loads in the event of a generator outage, solar PV outage, or depleted fuel reserves. While this work demonstrated an undesirable increase in carbon intensity in its results, the methods of weighting factor selection can be applied to prioritize this objective. Future work with the developed methodology can include application across different use cases with results used to compare and contrast weighting factor selection for varying priorities. Additionally, the algorithm can incorporate inputs for planned and unplanned maintenance of DERs to demonstrate how the controls approach can be used to schedule maintenance with least risk to critical loads.

Data availability statement

The datasets presented in this article are not readily available because the input data are information provided by the US DoD and would require permission to be given out to others upon request. The raw dataset showing outputs from the work developed are available upon request, however. Requests to access the datasets should be directed to mwodicke@asu.edu.

Author contributions

MW: Conceptualization, Formal Analysis, Investigation, Methodology, Project administration, Software, Validation, Visualization, Writing–original draft, Writing–review and editing. JN: Conceptualization, Investigation, Methodology, Writing–review and editing. NJ: Funding acquisition, Resources, Supervision, Writing–review and editing.

Funding

The author(s) declare financial support was received for the research, authorship, and/or publication of this article. Funding was provided in part by the US Department of Defense Environmental Security Technology Certification Program (ESTCP) under contract number W912HQ20C0051/ESTCP Project Number EW19-5367. ESTCP provided connections to stakeholders who gave input and data to inform analysis in the work.

Conflict of interest

The authors declare that the research was conducted in the absence of any commercial or financial relationships that could be construed as a potential conflict of interest.

Publisher's note

References

Abunima, H., and Teh, J. (2020). Reliability modeling of PV systems based on time-varying failure rates. *IEEE Access* 8, 14367–14376. doi:10.1109/access.2020.2966922

Anderson, J., and Bausch, C. (2006). Climate change and natural disasters: scientific evidence of a possible relation between recent natural disasters and climate change. *Policy Dep. Econ. Sci. policy* 2, 2.

Anderson, G. B., and Bell, M. L. (2012). *Lights out: impact of the August 2003 power outage on mortality in New York, NY*. Cambridge, Massachusetts: Epidemiology 23 (2), 189.

Ayar, M., Obuz, S., Trevizan, R. D., Bretas, A. S., and Latchman, H. A. (2017). A distributed control approach for enhancing smart grid transient stability and resilience. *IEEE Trans. Smart Grid* 8 (6), 3035–3044. doi:10.1109/tsg.2017.2714982

Bhattacharjee, V., and Khan, I. (2018). A non-linear convex cost model for economic dispatch in microgrids. *Appl. energy* 222, 637–648. doi:10.1016/j.apenergy.2018.04.001

Bhusal, N., Abdelmalak, M., Kamruzzaman, M., and Benidris, M. (2020). Power system resilience: current practices, challenges, and future directions. *IEEE Access* 8, 18064–18086. doi:10.1109/access.2020.2968586

Blanke, A. (2019). *California ISO 2018 annual report*. California, United States: California ISO.

Bruni, G., Cordiner, S., Mulone, V., Rocco, V., and Spagnolo, F. (2014). A study of energy management in domestic micro-grids based on model predictive control strategies. *Energy Procedia* 61, 1012–1016. doi:10.1016/j.egypro.2014.11.1013

Bryan, W. (2012). Emergency situation reports: hurricane sandy. *Off. Electr. Deliv. Energy Reliab. U. S. Dep. Energy, Hurric. Sandy Situat. Rep.* 20.

California ISO (2023). *California ISO – emissions, today's outlook*. California, United States: California ISO.

Cane, M. A., Clement, A. C., Kaplan, A., Kushnir, Y., Pozdnyakov, D., Seager, R., et al. (1997). Twentieth-century sea surface temperature trends. *science* 275, 957–960. 5302. doi:10.1126/science.275.5302.957

Cano, C. (2020). FERC opens wholesale markets to distributed resources: landmark action breaks down barriers to emerging technologies, boosts competition. *Fed. Energy Regul. Comm.*

Chen, T. M., Sanchez-Aarnoutse, J. C., and Buford, J. (2011). Petri net modeling of cyber-physical attacks on smart grid. *IEEE Trans. smart grid* 2 (4), 741–749. doi:10.1109/tsg.2011.2160000

Colli, A. (2015). Failure mode and effect analysis for photovoltaic systems. *Renew. Sustain. Energy Rev.* 50, 804–809. doi:10.1016/j.rser.2015.05.056

Derafshian, M., and Amjady, N. (2015). Optimal design of power system stabilizer for power systems including doubly fed induction generator wind turbines. *Energy* 84, 1–14. doi:10.1016/j.energy.2015.01.115

Dulău, L. I., Abrudean, M., and Bică, D. (2014). Effects of distributed generation on electric power systems. *Procedia Technol.* 12, 681–686. doi:10.1016/j.protcy.2013.12.549

Ellithy, K., Said, S., and Kahlout, O. (2013). "Design of power system stabilizers based on μ-controller for power system stability enhancement," in 2013 3rd International Conference on Electric Power and Energy Conversion Systems, Istanbul, Turkey, 2-4 October 2013 (IEEE).

Energy Government and US (2022). *Department of energy releases new tool tracking microgrid installations in the United States*. Washington DC: Energy.Gov, US Department of Energy.

EOS (2023a). *Eos aurora product description*.

EOS (2023b). EOS energy storage. Available at: https://eosenergystorage.com/.

Ericson, S. (2019). *Calculating the reliability of a backup system*.

ESSOM (2016). *Heating values of hydrogen and fuels*. Bangkok, Thailand: ESSOM CO. Ltd.

ESTCP (2019). *Data for ESTCP storage Program*. Washington, DC: Environmental Security Technology Certification Program ESTCP. Unpublished raw data.

Fu, Q., Nasiri, A., Solanki, A., Bani-Ahmed, A., Weber, L., and Bhavaraju, V. (2015). Microgrids: architectures, controls, protection, and demonstration. *Electr. Power Components Syst.* 43 (12), 1453–1465. doi:10.1080/15325008.2015.1039098

Fu, R., Feldman, D. J., and Margolis, R. M. (2018). *US solar photovoltaic system cost benchmark: Q1 2018*. Golden, CO (United States): National Renewable Energy Lab.NREL. No. NREL/TP-6A20-72399.

Gambirasio, G. (1976). Computation of loss-of-load probability. *IEEE Trans. Reliab.* 25 (1), 54–55. doi:10.1109/tr.1976.5214961

Golnas, A. (2012). "PV system reliability: an operator's perspective," in 2012 IEEE 38th Photovoltaic Specialists Conference (PVSC) PART 2, Austin, Texas, June 3-8, 2012 (IEEE).

Jafari, M., Malekjamshidi, Z., Zhu, J., and Khooban, M. H. (2018). A novel predictive fuzzy logic-based energy management system for grid-connected and off-grid operation of residential smart microgrids. *IEEE J. Emerg. Sel. Top. Power Electron.* 8 (2), 1391–1404. doi:10.1109/jestpe.2018.2882509

Johnson, N. (2022). *Design, modeling, and control of hybrid ESS for DoD microgrids*.

Kerr, R. A. (2011). "*Humans are driving extreme weather; time to prepare*." 1040–1040.

Khan, M. S., and Iravani, M. R. (2007). "Supervisory hybrid control of a micro grid system," in 2007 IEEE Canada Electrical Power Conference, Montreal, Canada, October 2007 (IEEE).

Khani, D., Ahmad, S. Y., and Hossein Madadi, K. (2012). Impacts of distributed generations on power system transient and voltage stability. *Int. J. Electr. Power & Energy Syst.* 43 (1), 488–500. doi:10.1016/j.ijepes.2012.06.007

Krismanto, A. U., Mithulananthan, N., Setiadi, H., Setyawan, E. Y., and Abdillah, M. (2021). Impacts of grid-tied microgrid on stability and interaction of power systems considering RE uncertainties. *Sustain. Energy, Grids Netw.* 28, 100537. doi:10.1016/j.segan.2021.100537

Lee, H. J., Niddodi, S., Srivastava, A., and Bakken, D. (2016). "Decentralized voltage stability monitoring and control in the smart grid using distributed computing architecture," in 2016 IEEE Industry Applications Society Annual Meeting, Portland, Oregon, 2-6 October 2016 (IEEE).

Ma, C., Kaufmann, P., Töbermann, J. C., and Braun, M. (2016). Optimal generation dispatch of distributed generators considering fair contribution to grid voltage control. *Renew. Energy* 87, 946–953. doi:10.1016/j.renene.2015.07.083

Meiqin, M., Meihong, J., Wei, D., and Chang, L. (2010). "Multi-objective economic dispatch model for a microgrid considering reliability," in The 2nd International Symposium on Power Electronics for Distributed Generation Systems, Hefei, China, 16-18 June 2010 (IEEE).

Miao, Z., Xu, L., Disfani, V. R., and Fan, L. (2013). An SOC-based battery management system for microgrids. *Ieee Trans. smart grid* 5 (2), 966–973. doi:10.1109/tsg.2013.2279638

Moretti, L., Polimeni, S., Meraldi, L., Raboni, P., Leva, S., and Manzolini, G. (2019). Assessing the impact of a two-layer predictive dispatch algorithm on design and operation of off-grid hybrid microgrids. *Renew. Energy* 143, 1439–1453. doi:10.1016/j.renene.2019.05.060

Mrowca, B. (2011). *Emergency diesel generator failure review 1999-2001*. Rockville Pike, MD, USA: Information Systems Laboratories, Inc.

Muir, A., and Lopatto, J. (2004). *Final report on the August 14, 2003 blackout in the United States and Canada: causes and recommendations*.

Nelson, J., Johnson, N. G., Fahy, K., and Hansen, T. A. (2020). Statistical development of microgrid resilience during islanding operations. *Appl. energy* 279, 115724. doi:10.1016/j.apenergy.2020.115724

Nelson, J. R., and Johnson., N. G. (2020). Model predictive control of microgrids for real-time ancillary service market participation. *Appl. Energy* 269, 114963. doi:10.1016/j.apenergy.2020.114963

Ogunjuyigbe, A. S. O., Ayodele, T. R., and Akinola, O. O. (2016). Impact of distributed generators on the power loss and voltage profile of sub-transmission network. *J. Electr. Syst. Inf. Technol.* 3 (1), 94–107. doi:10.1016/j.jesit.2015.11.010

Palma-Behnke, R., Benavides, C., Aranda, E., Llanos, J., and Sáez, D. (2011). "Energy management system for a renewable based microgrid with a demand side management mechanism," in 2011 IEEE symposium on computational intelligence applications in smart grid (CIASG), Paris, France, 11-15 April 2011 (IEEE).

Pecenak, Z. K., Stadler, M., and Kelsey, F. (2019). Efficient multi-year economic energy planning in microgrids. *Appl. Energy* 255, 113771. doi:10.1016/j.apenergy.2019.113771

Power, M. (2007). *750kW containerized diesel generator set*. Carson.

Raoufi, H., Vahidinasab, V., and Mehran, K. (2020). Power systems resilience metrics: a comprehensive review of challenges and outlook. *Sustainability* 12 (22), 9698. doi:10.3390/su12229698

Rawlings, J. B., and Mayne, D. Q. (2009). *Model predictive control: theory and design WI madison*. Santa Barbara, CA: Nob Hill Publishing.

Resource, MW Fault Induced Solar Photovoltaic (2017). *1,200 MW Fault Induced solar photovoltaic resource interruption disturbance report: southern California 8/16/2016 event*. Atlanta, GA: NERC.

Sherlock, M. F. (2018). *The energy credit: an investment tax credit for renewable energy*. Washington DC: Congressional Research Service, 7–5700.

Skoczek, A., Sample, T., Dunlop, E., and Ossenbrink, H. (2008). Electrical performance results from physical stress testing of commercial PV modules to the IEC 61215 test sequence. *Sol. Energy Mater. Sol. Cells* 92 (12), 1593–1604. doi:10.1016/j.solmat.2008.07.008

Stadler, M., and Naslé, A. (2019). Planning and implementation of bankable microgrids. *Electr. J.* 32 (5), 24–29. doi:10.1016/j.tej.2019.05.004

Stelloh, T. (2019). *California braces for more fires, blackouts as part of state's new 'normal.'*. New York, NY: NBC News.

Stott, P. (2016). How climate change affects extreme weather events. *Science* 352, 1517–1518. 6293. doi:10.1126/science.aaf7271

Sunrun Inc (2019). *Sunrun illustrates potential for home solar and batteries as wildfire mitigation solution*. San Fransisco, CA: Sunrun Inc. Available at: investors.sunrun.com/news-events/press-releases/detail/126/sunrun-illustrates-potential-for-home-solar-and-batteries.

The Climate Registry (2022). *The climate Registry 2022 default emission factor document*. Los Angeles, CA: The Climate Registry.

Theerthamalai, A., and Maheswarapu, S. (2010). An effective non-iterative "λ-logic based" algorithm for economic dispatch of generators with cubic fuel cost function. *Int. J. Electr. Power & Energy Syst.* 32 (5), 539–542. doi:10.1016/j.ijepes.2009.11.002

Thompson, C. C., Konstantinos Oikonomou, P. E., Etemadi, A. H., and Sorger, V. J. (2016). Optimization of data center battery storage investments for microgrid cost savings, emissions reduction, and reliability enhancement. *IEEE Trans. Industry Appl.* 52 (3), 2053–2060. doi:10.1109/tia.2016.2517149

Ton, D. T., and Smith, M. A. (2012). The US department of energy's microgrid initiative. *Electr. J.* 25 (8), 84–94. doi:10.1016/j.tej.2012.09.013

Unisdr, CRED. (2015). *The human cost of natural disasters: a global perspective*.

US Energy Information Administration (2022). *Weekly U.S. all grades all formulations retail gasoline prices (dollars per gallon)*. Washington DC: US Energy Information Administration.

Venkatasubramanian, V., and Yuan, Li. (2004). "Analysis of 1996 Western American electric blackouts," in *Bulk power system dynamics and control-VI* (Italy: Cortina d'Ampezzo), 22–27.

Wood, E. (2022). *Facebook and microsoft seed $50m fund for energy access microgrids*. Microgrid Knowledge.

Xiaoping, L., Ming, D., Jianghong, H., Pingping, H., and Yali, P. (2010). "Dynamic economic dispatch for microgrids including battery energy storage," in The 2nd international symposium on power electronics for distributed generation systems, Hefei, China, 16-18 June 2010 (IEEE).

Yu, M., Huang, W., Tai, N., Zheng, X., Wu, P., and Chen, W. (2018). Transient stability mechanism of grid-connected inverter-interfaced distributed generators using droop control strategy. *Appl. Energy* 210, 737–747. doi:10.1016/j.apenergy.2017.08.104

Zheng, A. (2022). *The untapped value of backup generation*. Morgantown, West Virginia: US Department of Energy.

Zhu, Y., Yan, J., Sun, Y., and He, H. (2014). Revealing cascading failure vulnerability in power grids using risk-graph. *IEEE Trans. Parallel Distributed Syst.* 25 (12), 3274–3284. doi:10.1109/tpds.2013.2295814

Appendix A

Mathematically optimized dispatch of microgrids requires analytical formulations to describe the behavior of the system and the intersectional relationship of decision variables. Table A1 includes the full list of constraints for grid-connected and islanded dispatch.

TABLE A1 Microgrid dispatch constraints.

Name	Constraint	Type of dispatch
Battery energy limit	$E_{bat}{}^{min} \le E_{bat,t} \le E_{bat}^{max} \quad for\, t = 0, ..., T_h \, and \, bat = 0, \ldots, N_{bat}$	Grid-connected, Islanded
Battery initial capacity	$E_{bat,0} = E_{bat}^{init} \quad for\, bat = 0, \ldots, N_{bat}$	Grid-connected, Islanded
Battery energy	$E_{bat,t} = E_{bat,t-1} + ((\eta_{bat} \times P_{bat,t-1}^{c}) - \frac{1}{\eta_{bat}}(P_{bat,t-1}^{d} + P_{bat}^{self})) \times \tau \quad for\, t = 1, ..., T_h \, and \, bat = 0, \ldots, N_{bat}$	Grid-connected, Islanded
Battery charge "Big M"	$P_{bat,t}^{c} \le B_{bat,t} \times M \quad for\, t = 0, \ldots, T_h \, and \, bat = 0, \ldots, N_{bat}$	Grid-connected, Islanded
Battery discharge "Big M"	$P_{bat,t}^{d} \le (1 - B_{bat,t}) \times M \quad for\, t = 0, \ldots, T_h \, and \, bat = 0, \ldots, N_{bat}$	Grid-connected, Islanded
Battery power charge limit	$P_{bat,t}^{c} \le P_{bat}^{c,max} \quad for\, t = 0, \ldots, T_h \, and \, bat = 0, \ldots, N_{bat}$	Grid-connected, Islanded
Battery power discharge limit	$P_{bat,t}^{d} \le P_{bat}^{d,max} \quad for\, t = 0, \ldots, T_h \, and \, bat = 0, \ldots, N_{bat}$	Grid-connected, Islanded
Generator power limit maximum	$P_{gen,t} \le P_{gen}{}^{max} \times B_{gen,t} \quad for\, t = 0, \ldots, T_h \, and \, gen = 0, \ldots, N_{gen}$	Grid-connected, Islanded
Generator power limit minimum	$P_{gen,t} \ge P_{gen}{}^{min} \times B_{gen,t} \quad for\, t = 0, \ldots, T_h \, and \, gen = 0, \ldots, N_{gen}$	Grid-connected, Islanded
Generator fuel use	$\frac{P_{gen,t}}{\eta_{gen} \times LHV_{fuel}} \times \tau \le F_t^{av} \quad for\, t = 0, \ldots, T_h \, and \, gen = 0, \ldots, N_{gen} \, and \, fuel = 0, \ldots, N_{fuel}$	Grid-connected, Islanded
Solar PV curtailment	$0 \le P_{sol,t} \le P_{sol,t}^{for} \quad for\, t = 0, \ldots, T_h \, and \, sol = 0, \ldots, N_{sol}$	Grid-connected, Islanded
Generator ramp-up rate	$P_{gen,t-1} - P_{gen,t} \le P_{gen}^{ramp,up} \quad for\, t = 1, \ldots, T_h \, and \, gen = 0, \ldots, N_{gen}$	Grid-connected, Islanded
Generator ramp-down rate	$P_{gen,t} - P_{gen,t-1} \le P_{gen}^{ramp,down} \quad for\, t = 1, \ldots, T_h \, and \, gen = 0, \ldots, N_{gen}$	Grid-connected, Islanded
Islanded controllable load	$P_{l,t}^{ctrl} = 0 \quad for\, t = 0, \ldots, T_h \, and \, l = 0, \ldots, N_{load}$	Islanded
Islanded power balance	$P_{gen,t} + (P_{bat,t}^{d} - P_{bat,t}^{c}) + P_{sol,t} - P_{l,t}^{crit} + P_t^{slack} = 0$ $for\, t = 0, \ldots, T_h \, and \, gen = 0, \ldots, N_{gen} \, and \, bat = 0, \ldots, N_{bat} \, and \, sol = 0, \ldots, N_{sol} \, and \, l = 0, \ldots, N_{load}$	Islanded
Grid buy "Big M"	$P_{grid,t}^{b} \le B_{grid,t} \times M \quad for\, t = 0, \ldots, T_h$	Grid-connected
Grid sell "Big M"	$P_{grid,t}^{s} \le (1 - B_{grid,t}) \times M \quad for\, t = 0, \ldots, T_h$	Grid-connected
Grid-connected power balance	$P_{gen,t} + (P_{bat,t}^{d} - P_{bat,t}^{c}) + P_{sol,t} + (P_{grid,t}^{b} - P_{grid,t}^{s}) - (P_{l,t}^{crit} + P_{l,t}^{ctrl}) = 0$ $for\, gen = 0, \ldots, N_{gen} \, and \, bat = 0, \ldots, N_{bat} \, and \, sol = 0, \ldots, N_{sol} \, and \, l = 0, \ldots N_{load}$	Grid-connected
TOU peak demand	$P_{grid,n}{}^{max} \ge P_{grid,t}^{b} \quad for\, t = 0, \ldots, T_h \, and \, n = 1, \ldots, N_{TOU} \quad when\, t_{TOU}^{b}(n) \le h(t) \le t_{TOU}^{e}(n)$	Grid-connected

Nomenclature

Symbol	Units	Description
A	hr	Duration of time a microgrid can serve 100% of critical load
α_{bat}	%	Battery stack availability
α_{gen}	%	Generator availability
α_{sol}	%	Solar photovoltaic availability
β^{tot}	mT CO_2	Total carbon intensity from serving microgrid load
b	N/A	Number of batteries stacks available as a subset of the total number of batteries stacks
b'	N/A	Number of batteries stacks available during the next system state
bat	N/A	Set of all battery stacks in microgrid
B_t^{slack}	N/A	Binary variable to describe when load is 100% served (1) or is curtailed (0) at simulation time step
$B_{bat,t}$	N/A	Binary variable to describe if a battery stack is charging (1) or discharging (0) at simulation time step
$B_{gen,t}$	N/A	Binary variable to describe if a generator is outputting power (1) or idle (0) at simulation time step
$B_{grid,t}$	N/A	Binary variable to describe if the point of common coupling is importing power (1) or exporting power (0) at simulation time step
$C_{bat}^{OM,v}$	/kWh	Variable operational cost of charging or discharging battery stack
$C_{grid,n}^{dem}$	/kW	Per-unit demand cost for time-of-use period
C^{OM}	$	Total annual operations and maintenance cost
$C_{grid,t}^{b}$	/kWh	Per-unit cost to buy energy from the utility at simulation time step
$C_{grid,t}^{s}$	/kWh	Per-unit price to sell energy to the utility at simulation time step
C_{grid}^{s}	$	Total annual revenue from energy sales
C^{total}	$	Total operating cost
C^{net}	$	Net operating cost
C_{gen}^{fuel}	/kWh	Per-unit fuel cost to operate generator
ϵ_{gen}	mT CO_2/MWh	Emissions factor for generator energy
ϵ_{grid}	mT CO_2/MWh	Emissions factor for utility energy
$E_{bat}{}^{min}$	kWh	Minimum energy capacity in a battery stack
E_{bat}	kWh	Total instantaneous energy capacity in all battery stacks during islanded operation
$E_{bat,t}$	kWh	Instantaneous energy capacity in battery stack at simulation time step
$E_{bat}{}^{max}$	kWh	Maximum energy capacity in battery stack
E_{bat}^{init}	kWh	Initial battery energy at the start of the time horizon
$E_{unserved}$	kWh	Total unserved energy for the microgrid during a utility islanding event
η_{bat}	%	Battery stack round-trip efficiency
η_{gen}	%	Generator efficiency
F_{gen}^{tot}	gallon	Total fuel consumed during a utility islanding event
F_t^{av}	gallon	Onsite fuel available at simulation time step
$fuel$	N/A	Set of all generator fuel types in microgrid
g	N/A	Number of generators within a subset of total generators
g'	N/A	Number of generators available in the next system state
gen	N/A	Set of all generators in microgrid
$h(t)$	N/A	Hour of the day at simulation time step
LHV_{fuel}	kWh/gallon	Lower heating value of diesel fuel
l	N/A	Number of loads within a subset of total loads
λ_{bat}	failure/hr	Failure rate of battery stacks
λ_{gen}	failure/hr	Failure rate of generators
λ_{sol}	failure/hr	Failure rate of solar photovoltaics
M	N/A	Any large number to be used in the "Big M" method, 1,000,000 in this work
N	N/A	Total possible combinations of assets available in microgrid portfolio
n	N/A	Set of all time-of-use periods in a microgrid rate structure
N_{bat}	N/A	Total number of battery stacks in microgrid portfolio
N_{fuel}	N/A	Total number of fuel types in microgrid portfolio
N_{gen}	N/A	Total number of generators in microgrid portfolio
N_{load}	N/A	Total number of loads in microgrid portfolio
N_{sol}	N/A	Total number of solar photovoltaics sources in microgrid portfolio
N_{TOU}	N/A	Number of time-of-use periods in utility rate structure
ω_{bat}	%	Objective function weighting factor for energy from battery stacks during islanded operation
ω_{fuel}	%	Objective function weighting factor for energy from fuel during islanded operation
ω_{load}	%	Objective function weighting factor for energy from unserved critical load during islanded operation
ω_{gen}	%	Objective function weighting factor for energy from onsite fuel reserve preservation during grid-connected operation
ω_{grid}	%	Objective function weighting factor for total operational cost during grid-connected operation
ω_{SOC}	%	Objective function weighting factor for energy from battery stack state of charge preservation during grid-connected operation
$P_{bat,t}^{c}$	kW	Charging power of battery at simulation time step
$P_{bat,t}^{d}$	kW	Discharging power of battery at simulation time step
$P_{bat}^{c,max}$	kW	Maximum power charge of battery stack
$P_{bat}^{d,max}$	kW	Maximum power discharge of battery stack
P_{bat}^{self}	kW	Discharge power of battery due to thermal energy loss
P_{gen}	kW	Total generator capacity

$P_{gen,t}$	**kW**	Output power of generator at simulation time step
P_{gen}^{max}	**kW**	Maximum output power of generator
P_{gen}^{min}	**kW**	Minimum output power of generator
$P_{gen}^{ramp,up}$	**kW/hr**	Generator ramp-up rate limit
$P_{gen}^{ramp,down}$	**kW/hr**	Generator ramp-down rate limit
$P_{l,t}^{crit}$	**kW**	Power consumption of critical load at simulation time step
$P_{l,t}^{ctrl}$	**kW**	Power consumption of controllable load at simulation time step
$P_{grid,n}^{max}$	**kW**	Peak demand during time-of-use period
P_{sol}	**kW**	Total solar photovoltaics capacity
$P_{sol,t}$	**kW**	Output power of solar photovoltaics at simulation time step
$P_{sol,t}^{for}$	**kW**	Forecasted solar PV at simulation time step
P_{t}^{tot}	**kW**	Total available generation capacity at simulation time step
$P_{grid,t}^{b}$	**kW**	Import power from the utility at simulation time step
$P_{grid,t}^{s}$	**kW**	Export power to the utility at simulation time step
P_{t}^{slack}	**kW**	Curtailed load during islanded operation at simulation time step
ρ_{gen}	**gallon/kWh**	Fuel conversion rate of the generator
Q	**N/A**	Statistical distribution of islanding events over the period of simulation
q_t	%	Probability of an islanding event to occur at simulation time step
s	**N/A**	Number of solar photovoltaics sources within a subset of total solar photovoltaics sources
s'	**N/A**	Number of solar photovoltaics sources available in the next system state
sol	**N/A**	Set of all solar arrays in microgrid
$S_h(t)$	%	Microgrid survivability at simulation time step
$\overline{S_h}$	%	Average microgrid survivability over the period of simulation
t	**N/A**	Current time step in the simulation time horizon
T	**N/A**	Transition matrix of for islanded operations
T_{bp}	**hr**	Total number of time steps in the utility billing period
T_h	**hr**	Total number of time steps in the simulation time horizon
T_{sim}	**hr**	Total number of time steps in the simulation
t_{TOU}^{b}	**N/A**	Beginning time step in a time-of-use period
t_{TOU}^{e}	**N/A**	Ending time step in a time-of-use period
τ	**hr/time** step	Time step hourly fraction
$u_{bat,t}^{c}$	**N/A**	Binary variable to describe unit commitment of battery charging at simulation time step
$u_{bat,t}^{d}$	**N/A**	Binary variable to describe unit commitment of battery discharging at simulation time step
$u_{gen,t}$	**N/A**	Binary variable to describe unit commitment of generator at simulation time step
$u_{sol,t}$	**N/A**	Binary variable to describe unit commitment of solar photovoltaics at simulation time step